Two Novel Relaxation Oscillator Interface Circuits for Resistive and Capacitive Sensors

by

Emily Hatfield

A thesis submitted to the Graduate Faculty of
Auburn University
in partial fulfillment of the
requirements for the Degree of
Master of Science

Auburn, Alabama
December 9, 2023

Keywords: Capacitive IDE Sensor, PCB Sensor, Relaxation Oscillator, Sensor Interface Circuit

Approved by

Robert N. Dean, Chair, McWane Professor of Electrical and Computer Engineering
Michael Baginski, Associate Professor
Thaddeus Roppel, Associate Professor Emeritus

Abstract

Presented in this thesis is the design and testing of two novel interface circuits for capacitive and resistive sensors. In both cases, the interface circuit is a modified CMOS inverter based relaxation oscillator, which correlates the sensor's capacitance/resistance to the fundamental frequency of its output square wave. Additionally, in both cases, the relaxation oscillator modulates the output signal onto the current signal of the power supply, which is recovered by a current transformer circuit at the power supply, obviating the need for a separate physical output signal connection. The first interface circuit is designed for use with a single resistive sensor. It is demonstrated with a thermistor that is evaluated via testing inside a freezer over a temperature range of 13 °C to -30 °C. Over that temperature range, the maximum error in the measured frequency of the oscillator interface circuit is 160 Hz. The second version uses two interface circuits, incorporating two capacitive sensors which are evaluated with a deionized water drop test. Both output signals are modulated onto the current signal of the power supply. The fundamental frequencies of the two relaxation oscillators are sufficiently different so that the output information from each interface circuit is recoverable by a frequency domain analysis of the current signal at the power supply. Both interface circuits demonstrate functionality and offer opportunities for further development and research.

Acknowledgements

Thank you, Dr. Robert Dean, for mentoring me and for teaching me to be a researcher. Thank you, Auburn University Department of Electrical and Computer Engineering, for teaching me to be an electrical engineer. Thank you, my family, for encouraging me, for loving me, and for inspiring me to become an engineer. Thank you, God, for blessing me with this opportunity and the people around me.

Table of Contents

List of Tables

List of Figures

Chapter 1

Introduction

Resistive and capacitive sensors are useful devices for monitoring environmental conditions, such as moisture content or temperature. As such, each sensor requires an interface circuit to read its changing resistance/capacitance and to translate that value into a comprehensible and analyzable quantity, such as a digital or analog signal. The interface circuit demonstrated in this work is a relaxation oscillator, which produces a periodic square wave created by the charging and discharging of a capacitor through a resistor that changes the state of a nonlinear circuit element.

One experiment utilizes an off-the-shelf thermistor in a relaxation oscillator to measure temperature. As the temperature shifts, the resistance of the thermistor changes, altering the period of the square wave produced by a novel relaxation oscillator that modulates the output oscillation onto the power supply current signal, eliminating the need for a separate signal connection in addition to the power and ground connections. By using a current transformer at the power supply, the square wave output signal of the relaxation oscillator passes to an op-amp circuit, which conditions it into a sufficient input for a microcontroller that reads and outputs the frequency of the square wave for analysis by the user.

A second experiment employs two capacitive fringing field sensors, each connected to a separate relaxation oscillator circuit. However, both oscillators utilize the same CMOS inverter chip and are designed to have significantly different fundamental frequencies. Because of this arrangement, the fundamental frequencies of both output square waves from the relaxation oscillators are distinguishable in the current signal returning to the power supply. Passing that returning current through a current transformer enables spectral analysis of the signal. Adding

moisture to the environment of each capacitive sensors, i.e. placing drops of deionized water on them, produces a quantifiable shift in its fundamental frequency peak in the spectral analysis, which can be analyzed by the user.

Chapter 2 presents relevant background information about capacitive fringing field sensors and relaxation oscillators. Chapter 3 details the design of both interface circuits, and Chapter 4 contains test procedures and collected data. Chapter 5 pertains to data analysis, and Chapter 6 concludes the work and presents avenues for further research.

Chapter 2

Background

2.1 Fringing-Field Capacitive Sensors

Capacitors have long found application as sensing devices due to their sensitivity to multiple physical and electrical properties. For example, Equation (2.1.1) describes the capacitance of a simple parallel-plate capacitor as

$$C = \varepsilon_r \varepsilon_0 \frac{A}{d} \tag{2.1.1}$$

where ε_r is the relative permittivity of the dielectric material between the two plates, ε_0 is the permittivity of free space, A is the area of overlap between the plates, and d is the distance between the plates. It should be noted that this equation for the capacitance between two plates is only valid for the condition $A >> d^2$. Otherwise, fringing effects must be taken into account. In that equation, the only constant is ε_0 – every other parameter may be altered to effect a change in the capacitance of the device. In order to adapt the parallel-plate capacitor into a sensor, the measurand must affect the overlap area of the plates, the distance between the plates, and/or the electrical permittivity of the material between the plates. However, the previous statement leads to a difficulty: the simple parallel-plate capacitor is an invasive sensor that must be in direct contact with a measurand, which produces disturbances in the test environment and possible distortions in the sensor readings [1]. Also, many realizations of miniaturized parallel-plate based sensors consist of mechanically fragile structures that can be easily damaged in the operating environment [2]. Consequently, for test cases that require undisturbed environments, researchers often utilize planar-electrode capacitive fringing-field sensors [3].

A capacitive fringing-field sensor is still a capacitive device, just like a parallel-plate capacitor, but it is structured differently so as to take advantage of the fringing fields between the

electrodes. In a traditional parallel-plate capacitor, most of the electric field is confined to the volume of space between the two plates and flows linearly from one plate to the other. A small portion of the electric field passes outside of the gap between the two plates and arcs from one plate to the other; that small portion is the fringing field. A capacitive fringing-field device is designed to maximize the amount of the electric field that is present in the fringing field. Since the fringing field arcs outside of the device structure, it is affected by changes in the electrical permittivity of the environment surrounding the device. Table 1 provides electrical permittivity values for some common materials.

Table 2.1.1: Relative Permittivity Values for Various Materials (Table adapted from Table E.2 "Properties for Selected Dielectrics" [4])

Material	Relative Permittivity (ε_r)
Air	1.0005
Glass	10
Silicon (pure)	11.8
Soil (dry)	3 – 4
Water (distilled, at approximately 20 °C [5])	81
Seawater	72

Thus, capacitive fringing-field sensors are noninvasive sensors. The configuration of such sensors depends greatly upon the application and the state of the art at the time of their conception.

As an early example, in the late 1980's, researchers interested in the relative permittivity of biological materials used the open end of a coaxial cable as a capacitive fringing-field sensor [6] [7]. [6] and [7] detail the designs and preliminary test results for different planar capacitors that attach to the open end of the cable in an effort to increase the overall capacitance, allowing the sensor to function at lower operational frequencies. In [6], the authors propose a multi-ring design while in [7], the authors put forward a banyan-tree design and a rising-sun design. In all

cases, the addition of an attached planar design to the coaxial cable increased the overall sensor capacitance as desired [6] [7].

For an example of a different application, two researchers proposed an accelerometer that relied upon a capacitive fringing-field sensor in 2003 [8]. Within the accelerometer, two beams suspended a dielectric proof mass above a planar capacitor with interdigitated electrodes (IDE) [8]. Figure 2.1.1 shows an example of an IDE structure.

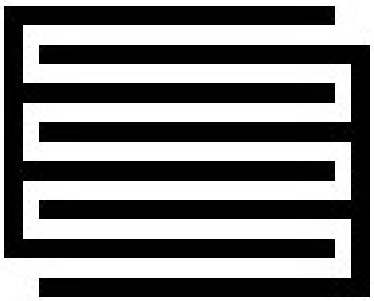

Figure 2.1.1: IDE Structure (Figure adapted from Figure 1 "A top-view illustration of two interdigitated electrodes." [9])

As applied forces caused the mass to ascend or descend over the planar capacitor, its changing position altered the electrical permittivity experienced by the fringing field of the capacitor, thus changing the capacitance of the device, from which the acceleration of the mass was inferred [8]. Although the accelerometer functioned under test, it suffered from insufficient sensitivity [8].

In 2008, two researchers proposed an alternative fringing-field sensor configuration [10]. The design was a cylinder with tapered ends; the two tapered ends were grounded electrodes while the middle of the cylinder was a separate, active electrode [10]. Thus, the fringing field arced from the middle section to the two outer portions [10]. The purpose of the device was to monitor the presence of water in stored agricultural goods such as wheat or corn; as such, the sensor could either be fixed in a container or attached to the end of a rod that could be manually inserted into a storage bin [10]. In testing, the sensor proved a functional success [10]. In particular, the authors noted its advantages over the more common planar IDE capacitive sensor

[10]. As the proposed sensor was larger than a typical planar IDE capacitive sensor, and its electrodes covered a larger surface area than the fingered electrodes of a typical IDE capacitive sensor, the proposed sensor had a greater sensitivity than typical IDE capacitive sensors of its time [10].

In 2010, a group of researchers evaluated the fitness of utilizing PCB technology to build planar IDE capacitive sensors [9]. The authors noted that PCB technology allows for the design of single or double-sided sensors [9]. Also, the solder mask can act as a protective barrier for the sensor, preventing potential shorting between the electrodes that might be caused by a conductive substance in the surrounding environment, such as water, while still being thin enough to allow the fringing fields of the sensor to interact with the environment outside the plane of the circuit board [9]. After manufacturing two PCB planar IDE capacitors and testing their abilities to sense varying amounts of water, the authors concluded that PCB technology was an appropriate medium for realizing low-cost planar IDE capacitive sensors [9].

An alternative technology for realizing capacitive fringing-field sensors is MEMS technology, which a team of researchers utilized in 2012 [11]. In their design, the sensor was composed of a mesh of electrodes [11]. In previous work, the authors determined that the effective edge lengths of the electrodes in the fringing-field sensor were more influential than the areas of the electrodes in increasing or decreasing the fringing field strength, so they applied that same principle to the design of their mesh sensor to optimally increase the strength of the fringing field [11]. In testing the sensor's responsiveness to temperature, the researchers found that their design proved functional [11].

In 2019, a team of researchers approached the design of moisture sensors for stored agricultural goods in an alternative method than the study described previously in [10]; they

opted to use a planar IDE capacitive sensor manufactured via PCB technology [12]. During testing, the researchers inserted the sensor into collections of corn kernels of varying moisture contents; the sensor did indicate the varying presence of moisture within the kernels but encountered sensitivity issues due to the irregular contact of the sensor surface with the corn kernels due to the kernels' variety of shapes [12]. But, the authors demonstrated the functionality of their sensor design and noted that it might compare favorably to IDE capacitive sensors fabricated via MEMS technology due to the relative size and cost differences [12].

One year later, another group of researchers also designed a moisture sensor using a fringing-field planar capacitive IDE sensor, but they used screen printing for fabrication rather than PCB technology [13]. The authors postulated that screen printing was less expensive than MEMS technology and less complicated than PCB fabrication [13]. In order to protect the electrodes from potential shorting due to environmental factors, the authors covered the electrodes with tape [13]. The authors tested the sensor by placing it in varying levels of water, and the sensor accurately demonstrated the measurement of changing water levels [13].

Likewise, in the same year, another group of researchers designed a fringing-field planar IDE capacitive sensor to measure liquid levels, but they fabricated their sensor by drawing it on paper with a graphite pencil [14]. They experimented with various thicknesses of paper and concentrations of graphite and concluded that increasing paper thickness and increasing concentration of graphite both corresponded to increasing capacitance [14]. Similarly to the researchers described in [13], these researchers also used tape to isolate the sensor from physical contact with the environment [14]. The sensor was intended for use inside syringes as a disposable method to monitor the amount of liquid medication dispensed [14]. The authors

evaluated the sensor's performance in that environment and concluded that the design demonstrated promise [14].

At this point, it is interesting to note the common usage of planar IDE capacitors as fringing-field sensors over a span of two decades. Although the planar IDE configuration is not suitable for every application, it is a proven design that functions well as a fringing-field capacitive sensor. Also, it is a design that is easily adapted for many different applications, and, depending on the technology used, it is a low-cost design to fabricate. For those reasons, the fringing-field capacitive sensor utilized in this work is a planar IDE capacitive sensor fabricated using low-cost commercial PCB technology. The capacitance of a planar IDE capacitive sensor is described in Equation (2.1.2) as

$$C \approx \frac{(n-1)\varepsilon_0\varepsilon_r A\gamma}{d} \tag{2.1.2}$$

where n is the number of electrode teeth, ε_0 is the permittivity of free space, ε_r is the relative permittivity of the substance in contact with the sensor surface, A is the overlapping tooth area of adjacent teeth, γ is a fringing-field scale factor where $\gamma \geq 1$, and d is the distance between adjacent teeth [9]. In this work, the planar IDE capacitive sensor functions as a moisture sensor.

2.2 Relaxation Oscillators

The relaxation oscillator is an interface circuit for resistive, capacitive, and inductive sensors. In essence, the oscillator produces an oscillating waveform, the period of which is determined by the resistive and capacitive/inductive elements in the circuit. As the capacitive or inductive elements store and dissipate charge, the rate at which they do so depends mainly upon two factors: their own capacitances/inductances and the resistances that the circuit presents to them. Altering any of these values changes the period of the oscillating waveform. As this is the case, if any of the capacitors, inductors, or the dominant resistor is a sensing element, then

changes in the value of the sensor result in an altered period of oscillation. Thus, changes in the environment are quantified as changes in the oscillation period of the signal; those changes can be analyzed, which is the goal of a sensor interface circuit. Relaxation oscillators have the additional advantage of being highly adaptable in design, as shown in the following examples.

A standard implementation of a relaxation oscillator in CMOS technology is shown in Figure 2.2.1.

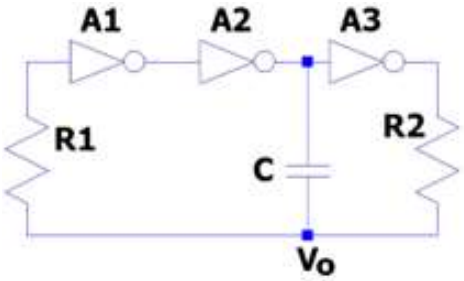

Figure 2.2.1: Standard CMOS Relaxation Oscillator (Figure adapted from Figure 2 "Basic CMOS inverter relaxation oscillator circuit." [15])

R1, R2, and C are all additions to a basic ring oscillator, the oscillation frequency of which is determined by

$$f = \frac{1}{2n\tau_D} \tag{2.2.1}$$

where *n* is the odd number of inverters, and τ_D is the propagation delay of an inverter [15]. The addition of R1, R2, and C incorporates a first order network into the ring oscillator so that the frequency of oscillation no longer depends upon inverter delay but upon the rate at which the capacitor charges and discharges. If R2 and C are sized appropriately so as to form the longest time constant in the circuit, and if the inverters are identical and change state at half of the power supply voltage, then the transfer function for the circuit can be represented as

$$\frac{V_o}{V_s} = \frac{R_2}{R_2 + \frac{1}{sC}} = \frac{s}{s + \frac{1}{R_2 C}}$$

where

$$V_s(s) = \frac{7.5}{s}.$$

It follows that

$$V_o(s) = V_s(s)\left(\frac{s}{s + \frac{1}{R_2C}}\right) = \frac{7.5}{s + \frac{1}{R_2C}}$$

which is equivalent to

$$V_o(t) = 7.5e^{-\frac{t}{R_2C}}.$$

Solving for the time at which the inverters change state yields

$$t = 1.0986R_2C$$

which is half of the oscillation period. Thus, the frequency of the circuit in Figure 1 can be represented as

$$f = \frac{1}{2t} \cong \frac{0.455}{R_2C}\ [16]. \qquad (2.2.2)$$

However, not all relaxation oscillator designs are based upon the ring oscillator.

In 1984, a researcher described the operation and governing equations of a relaxation oscillator based upon a 555 timer chip [17]. The timer chip was composed of two comparators connected to a set-reset flip-flop; the output of one comparator connected to the set pin of the flip-flop, and the output of the other comparator connected to the reset pin of the flip-flop [17]. The flip-flop's inverted output connected to the base of a BJT, which controlled the flow of current to a capacitor [17]. The voltage across that capacitor then fed back to the inputs of the comparators [17]. So, the comparators' outputs determined whether the flip-flop output was set or reset, which in turn controlled whether the transistor was on, allowing current flow, or off, prohibiting current flow [17]. When current was flowing, the capacitor charged, raising the

voltage across it, and when current was not flowing, the capacitor discharged, lowering the voltage across it [17]. Finally, when the voltage across the capacitor had risen or lowered to a sufficient level, the outputs of the comparators changed, flipping the state of the flip-flop output, which then swapped the state of the transistor and the build-up or depletion of charge at the capacitor [17]. The alternating raising and lowering of voltage at the capacitor created the oscillating output waveform [17]. The author explained that the 555 timer chip could be configured to either create a single pulse or a continuous oscillation and derived some basic design equations for generating a waveform of a particular frequency with the device [17].

In 1990, a team of researchers designed a relaxation oscillator with an output intended to interface well with a digital system [18]. Their oscillator consisted of a comparator and an integrator connected together by capacitors, which transferred charge between the two devices, creating the oscillation [18]. The duty cycle of the oscillating waveform depended upon the ratio between two capacitors [18]. The authors proposed that one of those capacitors be a sensor while the other be a reference so that by analyzing the duty cycle of the output, the data from the sensor might be recovered [18]. After testing the circuit in computer simulation, the authors concluded that it functioned as desired and produced an output usable by digital systems [18].

A different team of researchers created a temperature compensation scheme for oscillators based upon the bipolar junction transistor (BJT) [19]. The paper addressed two popular BJT oscillator designs, the Schmitt-trigger oscillator and the multivibrator [19]. The Schmitt-trigger oscillator relied upon a differential pair of BJTs that alternately switched on and off, controlling the flow of current across a capacitor, which created an oscillating voltage as the capacitor charged and discharged [19]. The authors determined that a large source of temperature dependence for the Schmitt-trigger oscillator was the hysteresis voltage of the transistors and

added circuitry to compensate [19]. The multivibrator was an oscillator that used two sets of cross-coupled BJTs to control the alternate charging and discharging of a capacitor; importantly, the voltage across the capacitor was limited by clamping diodes, so the temperature dependences of the diodes created an overall temperature dependence for the entire circuit [19]. The authors used a similar compensation scheme for the multivibrator as the one used for the Schmitt-trigger oscillator [19]. Computer simulations and fabrication of the proposed design demonstrated the relative temperature independence of the circuits [19].

In 2000, a group of researchers analyzed the behavior of a relaxation oscillator composed of an op-amp integrator and a comparator [20]. Firstly, they tested the relationship between capacitance and the period of oscillation by substituting different capacitance values into the circuit and measuring the period of oscillation [20]. Upon discovering that the relationship was not entirely linear, as previously expected, the researchers explored the non-ideal effects of the op-amp and comparator upon the circuit [20]. They concluded that the uncertainties of the response delays of the comparator and the imprecise characterization of small capacitances influenced the above-mentioned nonlinearity [20].

A different relaxation oscillator was proposed in 2010 for the purpose of providing a low power clock for battery-powered devices [21]. The oscillator was composed of a capacitor, a comparator, a switch, an SR flip-flop, a current generator, a voltage regulator, and a clock divider [21]. The current generator charged the capacitor until its voltage reached the necessary threshold to invert the output of the comparator, which signaled the flip-flop to close the switch temporarily and discharge the capacitor [21]. Then, the switch opened, and the capacitor began to charge again; repetition of that cycle created the oscillation [21]. The voltage regulator and clock divider processed the oscillating signal into a usable clock signal [21]. Additionally, the

oscillator was designed to be resistant to the influences of temperature upon the output signal [21]. Under test, the design proved functional and was minimally affected by temperature over a given range [21].

In 2012, a different group of researchers created a relaxation oscillator to interface with a pressure sensor [22]. They used the same oscillator design as that used in [21] [22]. A voltage reference and a capacitor, both fed by a bias current, formed the two inputs into a comparator; when the voltage across the charging capacitor surpassed the reference, the comparator output changed states [22]. The changed output forced a switch across the capacitor to close, discharging the capacitor and changing the comparator output state yet again [22]. The circuit continued in this manner, forming an oscillator [22]. The designers noted that the oscillator was low power, CMOS compatible, and functional across a variety of temperatures [22].

In 2013, two researchers demonstrated interfacing a relaxation oscillator with a frequency-locked loop (FLL) [16]. The relaxation oscillator was a modified ring oscillator that incorporated a capacitive sensor [16]. The charging and discharging of the capacitive sensor controlled the timing of the state change of the inverters, thus setting the frequency of the oscillating waveform [16]. The FLL received the oscillator's output as its input and matched its frequency; then, the loop assigned a digital word to that frequency value [16]. Thus, as the capacitive sensor changed value, the digital word also changed, providing the researchers with a simpler method to analyze the behavior of the sensor [16]. In testing, the researchers verified that the proposed design functioned by experimentally discovering a linear relationship between the capacitance of the sensor and the value of the digital word, as expected [16].

In 2015, a group of researchers designed a relaxation oscillator that connected to a center tap transformer [23]. The relaxation oscillator connected to the primary winding of the

transformer so that the secondary winding reproduced the oscillating waveform in its original phase and 180° out of phase [23]. Then, both waveforms passed to capacitors, each of which connected to an arm of the transformer and to the other capacitor; one capacitor was a capacitive sensor while the other capacitor was a reference capacitor [23]. The output current of the capacitors was converted to a voltage and then passed to the input of the relaxation oscillator, which consisted of an integrator and a comparator [23]. Finally, the output of the relaxation oscillator connected back to the primary winding of the transformer [23]. By so designing the circuit, the researchers hoped to obviate the effect of any parasitic capacitances to ground [23]. The researchers used experimentation to confirm the functionality of the design and simulation to confirm the design's imperviousness to the effects of parasitic capacitance to ground [23].

Five researchers proposed a relaxation oscillator design in 2016 for low power applications [24]. Their design combined two oscillators and two current sources [24]. The primary oscillator produced the desired output signal; the secondary oscillator controlled the current sources to produce a boosted current at particular times to negate the effects of the comparator's phase delay upon the period of the primary oscillation [24]. Additionally, the primary oscillator utilized a differential structure in order to eliminate the influence of any offset voltage created by the comparator [24]. In simulation, the proposed design demonstrated temperature stability comparable to that of other previous designs for low power oscillators, albeit over a smaller temperature range than some of the previous designs [24].

In 2019, another group of researchers proposed yet another design for a relaxation oscillator [25]. In their design, a comparator drove a set-reset latch (SR) [25]. The inputs of the comparator were the resistive and capacitive elements that determined the time constant of the oscillation, arranged differentially [25]. The differential arrangement included several switches,

controlled by the outputs of the set-reset latch, for switching in/out different capacitors to lower the phase noise of the oscillator [25]. In simulations, the proposed design demonstrated low phase noise and temperature stability [25].

As shown in the above examples, the relaxation oscillator is a valid interface circuit for capacitive, inductive, and resistive sensors. Additionally, it is a circuit with a highly flexible design, adaptable to many different sensors and applications. For this project, the relaxation oscillator utilized is a modified CMOS ring oscillator, the design of which will be discussed in the following sections.

Chapter 3

Design

3.1 Thermistor Interface Circuit

3.1.1 Relaxation Oscillator Design

In this project, the relaxation oscillator used is a modified ring oscillator, as shown in Figure 3.1.1.1.

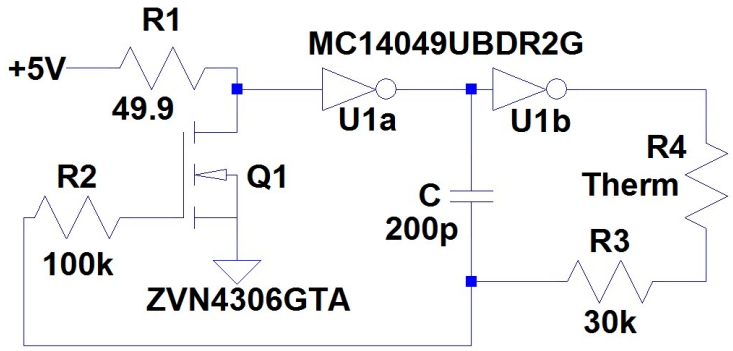

Figure 3.1.1.1: Relaxation Oscillator Circuit Diagram [15]

Initially, the NMOS transistor is in an off state, resulting in a drain voltage that is roughly equivalent to the supply voltage +5V (logically 'high') and no drain current. Consequently, the inverters set the voltage at the output of U1a to be logically 'low' and the voltage at the output of U1b to be 'high'. The 'high' voltage at the output of U1b results in current flow through resistors R4 and R3 that charges the capacitor C, increasing the voltage at node connecting C to R3 and R2. Because there is no appreciable current flow through resistor R2 into the gate of the transistor, the voltage at the node connecting C to R3 and R2 is approximately equivalent to the voltage at the gate of the transistor. Thus, when the voltage at that node reaches a sufficient level, the transistor turns on, dropping the voltage at the drain to a 'low' state and creating a drain current. Then, the inverters push the voltage at the output of U1a 'high' and the voltage at the output of U1b 'low'. The capacitor begins to discharge via current flow through resistors R3 and

R4, lowering the voltage at the node connecting C to R3 and R2. When the voltage at that node decreases to a value insufficient to keep the transistor on, the transistor shuts off, raising the drain voltage back to ‘high’ and preventing drain current flow. At that point, the process repeats cyclically, creating an oscillating waveform present in voltage and current signals. It is important to note that the oscillating waveform is present in a current signal because of the switching on and off of Q1, which significantly raises the amount of current drawn by the circuit when Q1 is on and lowers the amount of current drawn by the circuit when Q1 is off. That behavior superimposes the oscillation onto the current signal from the power supply; because of this feature, the circuit uses more power than a traditional CMOS inverter chip relaxation oscillator. In this operation, the period of oscillation arises from the RC time constant created by the resistive and capacitive elements. Additionally, if either resistors R3 or R4 or capacitor C1 is a sensing element, then changes in the resistance/capacitance of the sensor result in an altered period of oscillation. Thus, changes in the environment are quantified as changes in the period of a signal, which can be analyzed, accomplishing the goal of a sensor interface circuit.

The physical relaxation oscillator is shown in Figure 3.1.1.2, the back of the relaxation oscillator is shown in Figure 3.1.1.3, and an unpopulated board for the relaxation oscillator is shown in Figure 3.1.1.4.

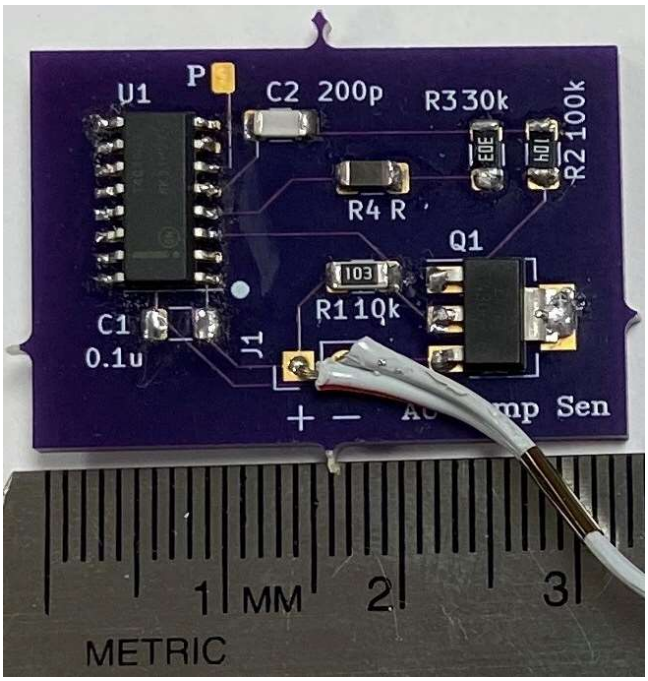

Figure 3.1.1.2: Relaxation Oscillator [15]

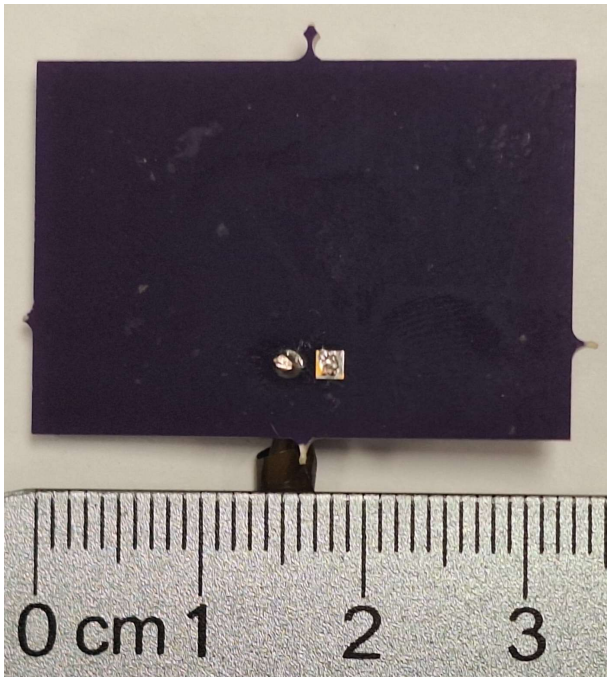

Figure 3.1.1.3: Relaxation Oscillator Back

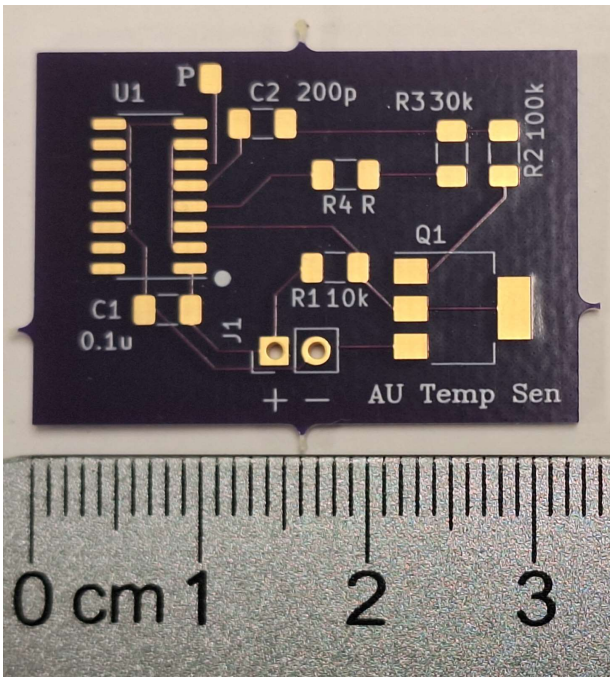

Figure 3.1.1.4: Unpopulated Relaxation Oscillator

The physical oscillator is a 2 layer PCB with an FR-4 substrate, fabricated by the company Osh Park [26]. The oscillator resistor R4 is a Kyocera NC20K00103JBA thermistor [27]. The CMOS inverters are located on the MC14049UBDR2G chip, labeled in Figure 3.1.1.2 as U1, and all of the unused inverter inputs on the chip are grounded [28][29]. Point P in Figure 3.1.1.2 is a signal probe point that connects to an inverter acting as a signal buffer. The NMOS transistor is the ZVN4306GTA [30]. C1 is a location for an optional decoupling capacitor for the CMOS inverter chip; the decoupling capacitor was not needed and thus not included. A 2 wire ribbon cable, seen in Figure 3.1.1.2 as covered in gray sleeving, connects the oscillator to the power supply, a Hewlett Packard E3610A DC power supply [31][32]. The GND wire in the ribbon cable passes through the current transformer, a Bergoz CT-B1.0-B [33][34], which reads the changing ground current and transforms that current into a representational voltage signal that is supplied to the op-amp circuit. Figure 3.1.1.5 shows the current transformer, and Figure 3.1.1.6 shows the voltage signal produced by the current transformer.

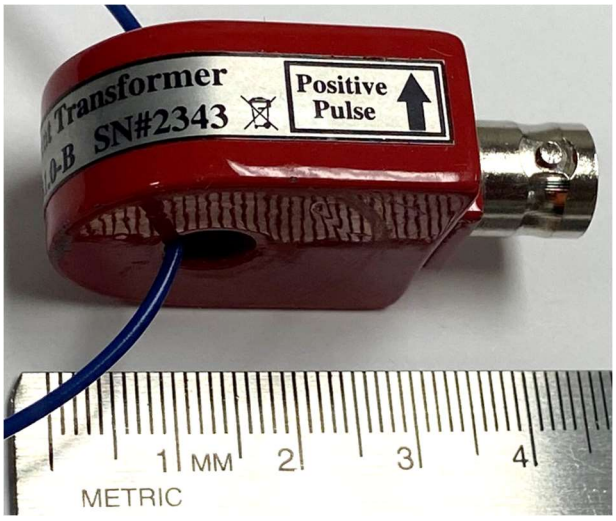

Figure 3.1.1.5: Current Transformer [15]

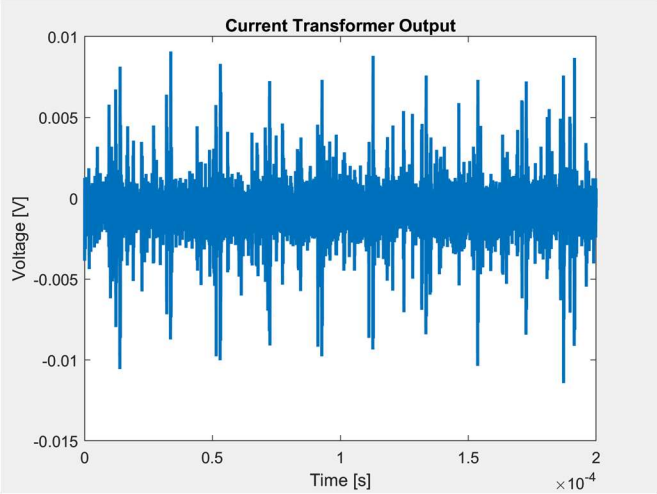

Figure 3.1.1.6: Output Signal of Current Transformer [15]

3.1.2 Current Transformer Circuit Design

The voltage waveform produced by the current transformer passes to an op-amp circuit in order to properly condition it before it flows to the microcontroller. Figure 3.1.2.1 is a circuit diagram of the op-amp circuit.

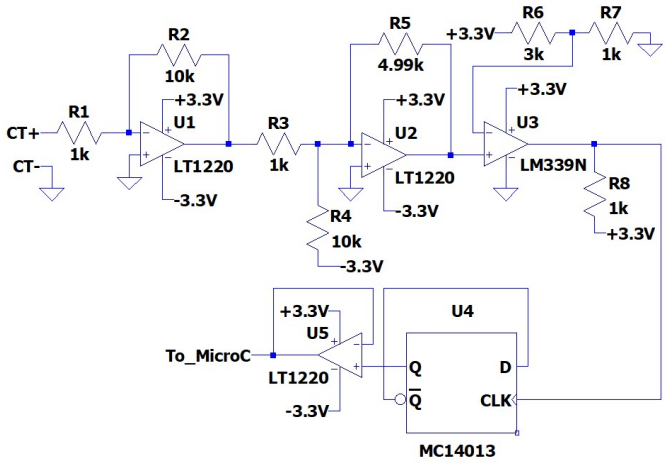

Figure 3.1.2.1: Current Transformer Circuit Diagram [15]

The op-amp circuit consists of two cascaded inverting amplifiers (LT1220) that enlarge the signal to an appropriate level for the following comparator. The first amplifier stage has an approximate gain of -10 V/V, and the second amplifier stage has an approximate gain of -5 V/V. Figure 3.1.2.2 is an example of the signal at the output of the two amplifiers.

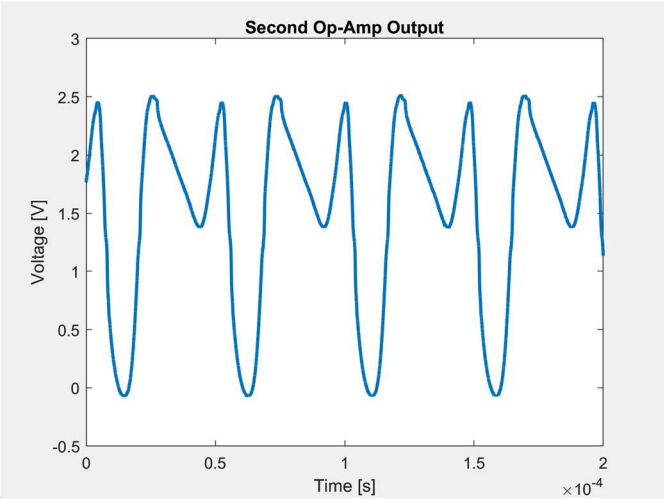

Figure 3.1.2.2: Output Signal of Cascaded Amplifiers [15]

The comparator eliminates the smaller spikes and produces a square wave, which then passes to the D flip-flop. Figure 3.1.2.3 shows the signal at the output of the comparator (LM339N).

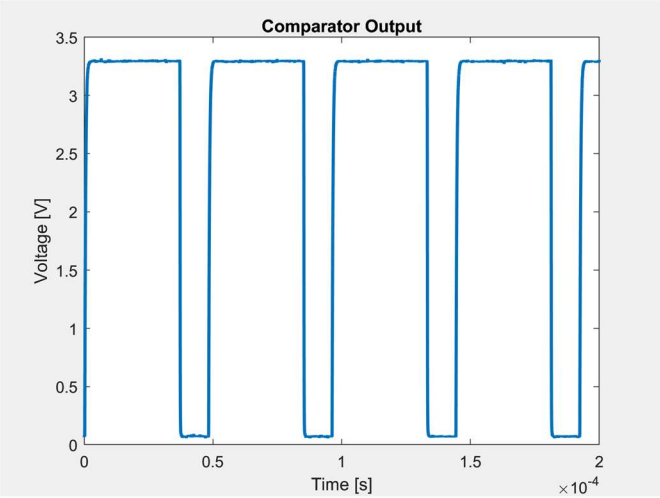

Figure 3.1.2.3: Output Signal of Comparator [15]

The D flip-flop lowers the signal frequency and adjusts the duty cycle to 50 percent, as shown in Figure 3.1.2.4.

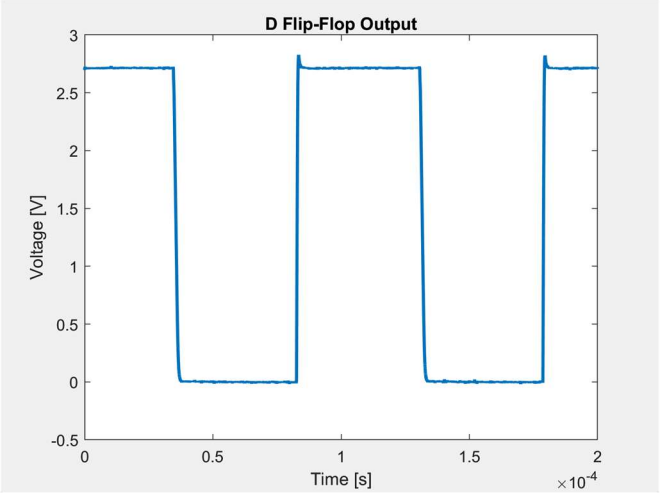

Figure 3.1.2.4: Output Signal of D flip-flop [15]

Then, the signal passes through a voltage buffer and travels to the microcontroller input.

The circuit, which exists in breadboard form, is shown in Figure 3.1.2.5.

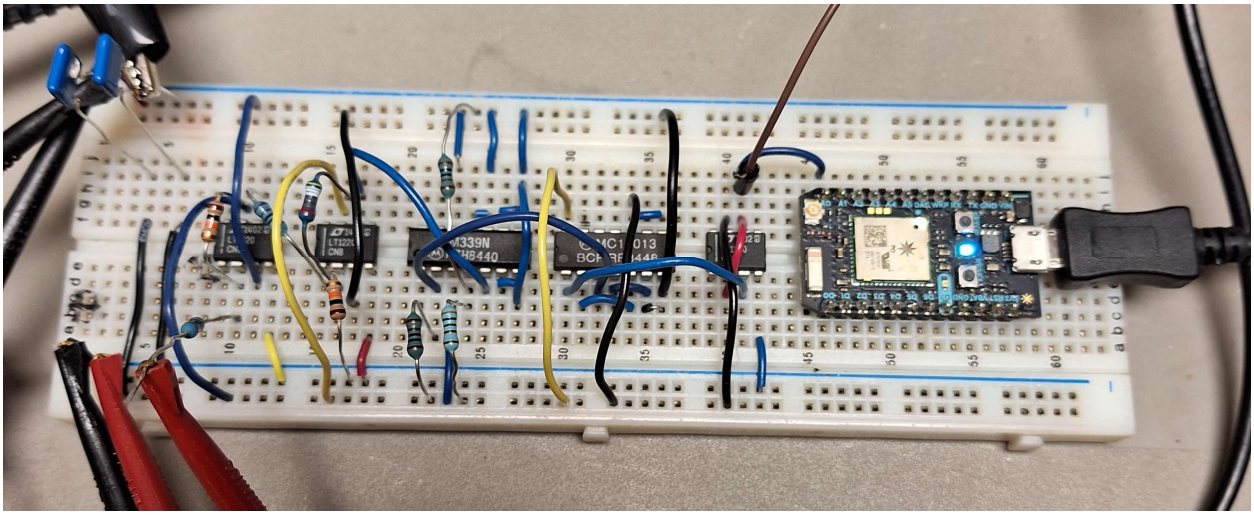

Figure 3.1.2.5: Breadboarded Current Transformer Circuit

It utilizes an Agilent E3631A triple output DC power supply [35]. Two ceramic capacitors, both approximately 1.7 µV, act as shunts from the + 3.3 V/– 3.3 V supply rails to GND to reduce any noise contamination from the power supply. All of the op-amps are LT1220's [36][37]. The comparator is a LM339N [38][39], and the D flip-flop used is a part of a MC14013 chip [40].

3.1.3 Microcontroller Code Design

The microcontroller used is the Particle Photon (shown on the right end of the breadboard in Figure 3.1.2.5), and it is powered via a USB cable connection to a computer [41][42]. The project's code was created and is stored on the Particle Web integrated development environment (IDE), which uses a similar syntax to the Arduino IDE. From the Particle Web IDE, the Photon downloads code via a Wi-Fi connection and then stores and runs the code until it is turned off or instructed to download new code. If the device is powered off and then powered on at a later point, the Photon will resume the code that it was previously running.

The signal output from the op-amp circuit is read at a general-purpose input/output (GPIO) pin on the microcontroller. The microcontroller measures the low pulse of the input waveform and calculates the waveform's frequency. Then, it prints that value via a WiFi

connection to an online user portal. For reference, the microcontroller code is presented in Appendix A.

3.2 Capacitive Sensors Interface Circuit

3.2.1 PCB Capacitive Sensors Design

Figure 3.2.1.1 is the CAD drawing of the PCB capacitive sensors used in this circuit, and Figure 3.2.1.2 shows the physical sensors.

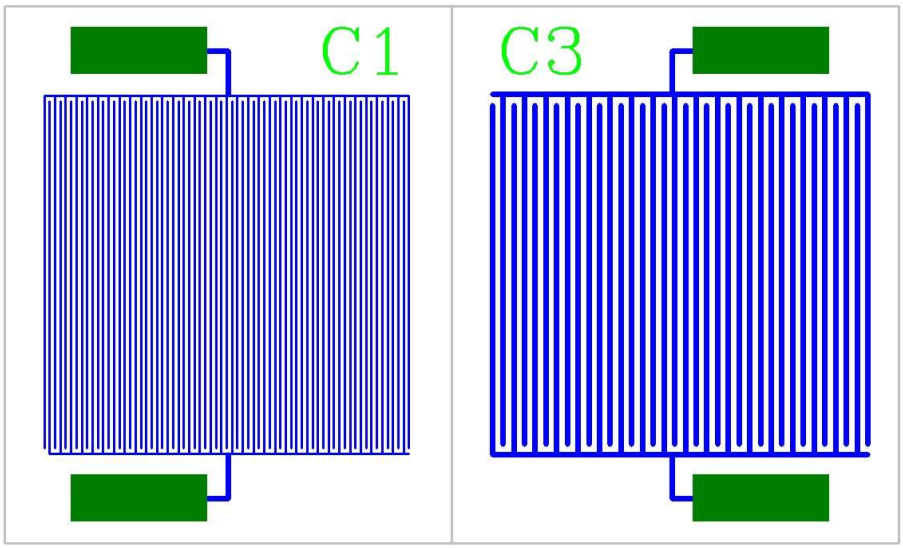

Figure 3.2.1.1: PCB Capacitive Sensors CAD Drawing

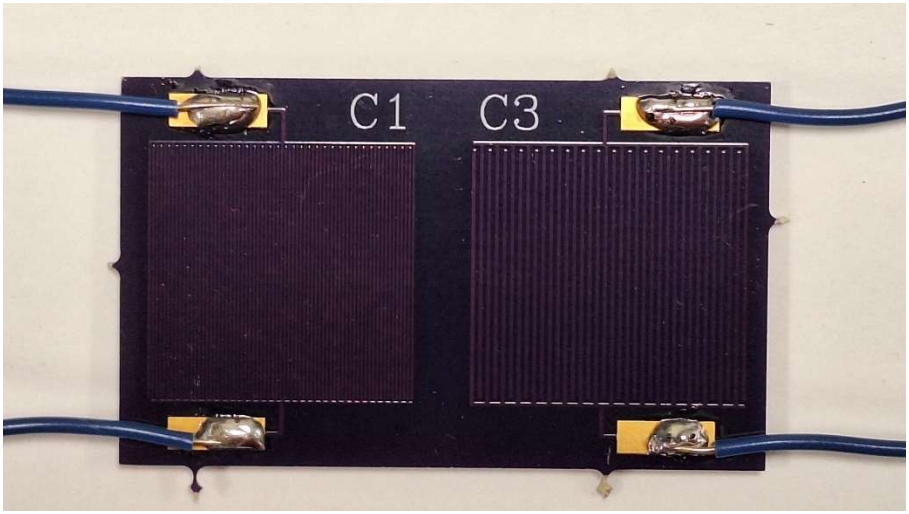

Figure 3.2.1.2: PCB Capacitive Sensors

The PCB consists of 2 separate capacitive IDE sensors and is a 2 layer board with an FR-4 substrate, also fabricated by Osh Park [26]. The capacitor labeled C1 in Figure 3.2.1.2 has 69 interdigitated fingers, with 34 attached to the bottom electrode and 35 attached to the top, and uses 6 mil space and trace. The capacitor labeled C3 in Figure 3.2.1.2 has 36 interdigitated fingers, with 18 attached to each electrode, and uses 12 mil space and trace. The entire structure, except for the conductive pads to which leads are soldered, is covered in polymeric solder mask.

3.2.2 Relaxation Oscillators Design

The circuit diagram of the relaxation oscillators utilized in this work is shown in Figure 3.2.2.1. The physical circuit is shown in Figure 3.2.2.2, in which the long blue leads that connect the capacitive sensors to the circuit extend beyond the frame of the photo. Although the circuit architecture is the same as in the circuit shown in Figure 3.1.1.1, R2 and R5 are significantly different from each other in order to produce output square waves with significantly different fundamental frequencies. This difference in fundamental frequencies allows the two output signals to be differentiated by spectral analysis of the current signal from the power supply.

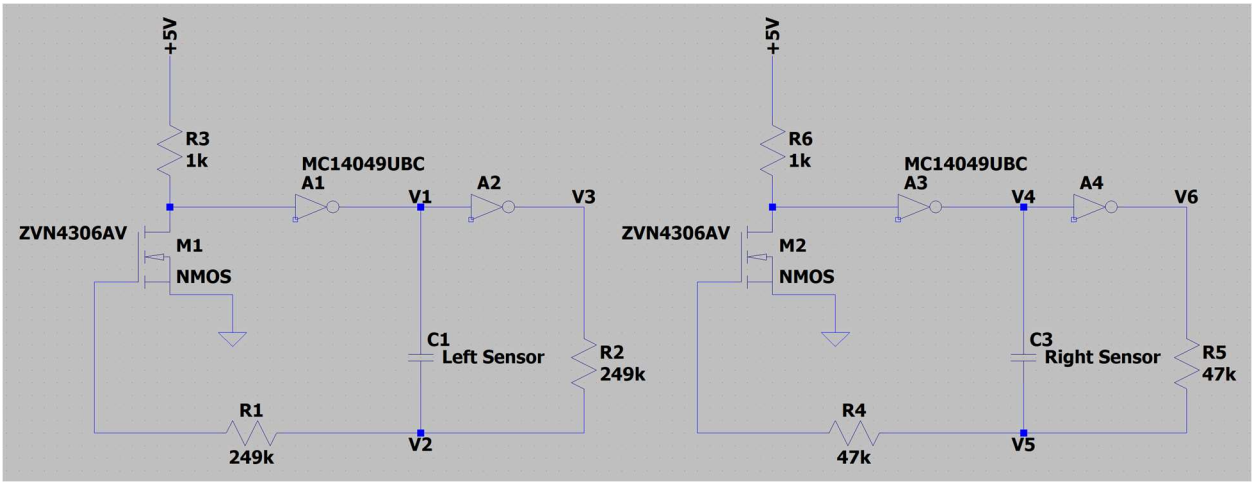

Figure 3.2.2.1: Relaxation Oscillators Circuit Diagram

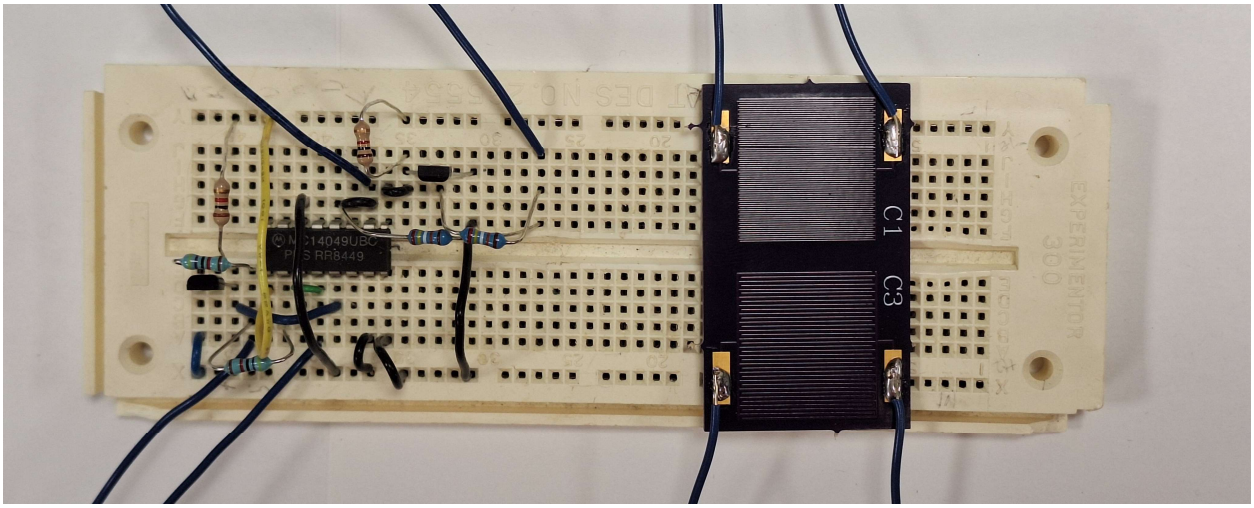

Figure 3.2.2.2: Relaxation Oscillator Circuit

The oscillator capacitors are the PCB capacitive sensors shown in Figure 3.2.1.1. The CMOS inverters are located on a single MC14049UBC chip [28]. All of the unused inverter inputs on the inverter chip are grounded. The NMOS transistors are ZVN4306AV's [43]. The physical circuit exists on a breadboard and connects via wires to a Hewlett Packard E3610A DC power supply [31]. The wire connected to the GND terminal of the power supply passes through the current transformer, a Bergoz CT-B1.0-B [33], which reads the changing ground current and produces a representational voltage waveform that is fed into a digital oscilloscope, a DSO-281OR manufactured by Virtins Technology [44]. Figure 3.2.2.3 shows the representational voltage waveform produced by the current transformer.

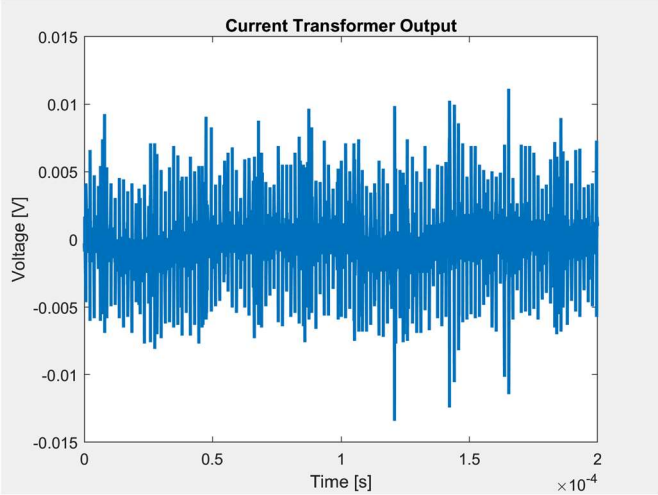

Figure 3.2.2.3: Output Signal of Current Transformer for 2 Oscillators

Chapter 4

Test Procedure and Data

4.1 Thermistor Interface Circuit Test

The functionality of the circuit design was tested by putting the oscillator PCB and a thermocouple into a Revco Scientific Inc. ULT350-5-A12 freezer. The test setup is shown in Figure 4.1.1. Figure 4.1.2 shows the position of the sensor board and the thermocouple inside the freezer where the thermocouple lead is the blue wire attached to the back of the sensor board.

Figure 4.1.1: Thermistor Interface Circuit Test Setup

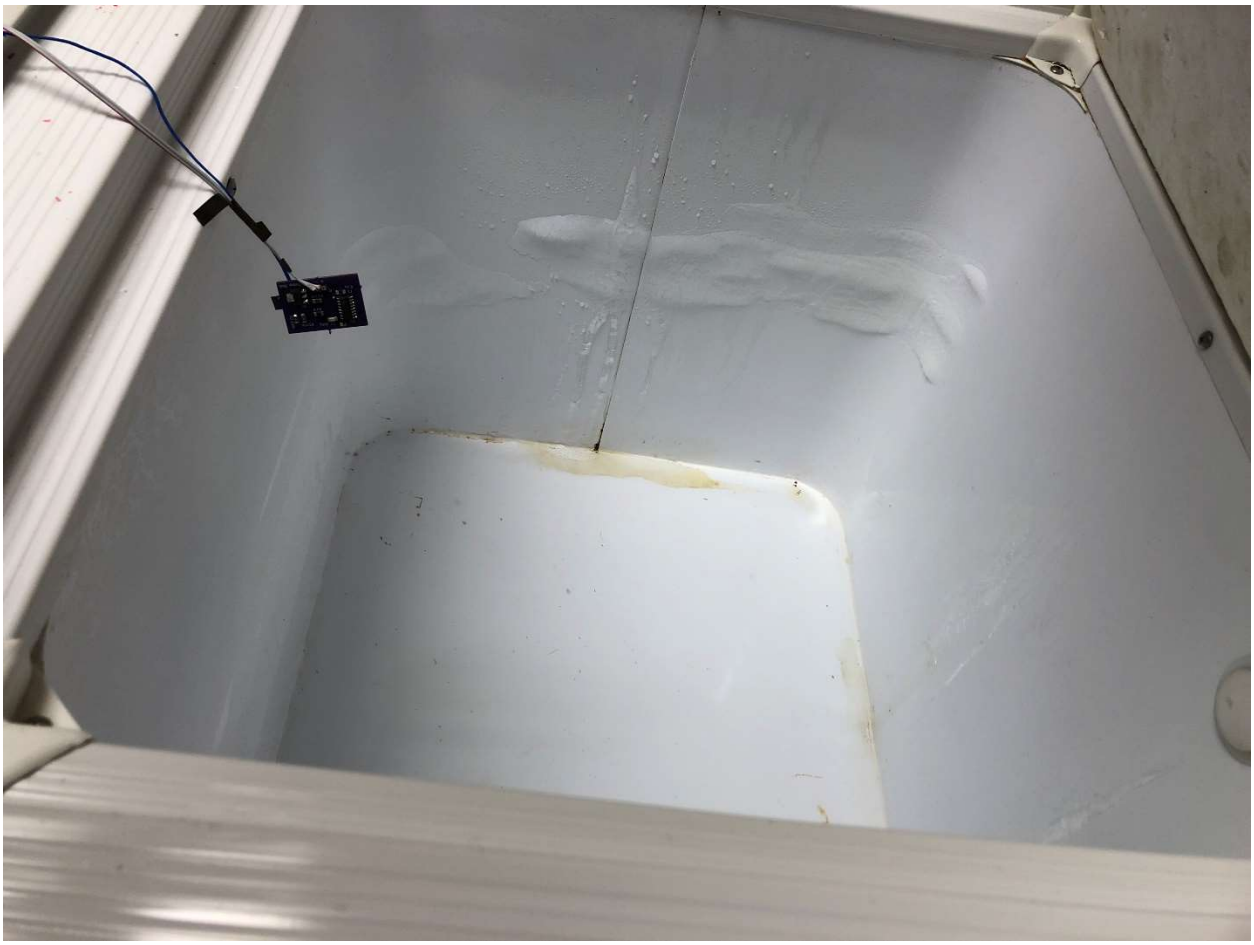

Figure 4.1.2: Thermistor Sensor Board inside Freezer

Running the cables of the oscillator and thermocouple through the seal surrounding the freezer lid enabled the connection of both to their respective equipment, the thermocouple to a meter and the oscillator to its associated circuitry as described in section 3.1. Those connections allowed the examination of the freezer's internal temperature and the relaxation oscillator's oscillation frequency in real time. Lowering the temperature inside the freezer increased the resistance of the thermistor in the oscillator circuit, which resulted in a lower oscillation frequency.

For the test, the freezer temperature was lowered from 13 °C to -30 °C as measured by the thermocouple. The oscillation frequency was calculated by the microcontroller as described in section 3.1 and, additionally, was measured by an oscilloscope at the output of the voltage

buffer. The data from the test is presented in Table 4.1.1 where Δ Frequency is the oscilloscope frequency subtracted from the microcontroller frequency.

Table 4.1.1: Thermistor Freezer Test Results			
Temp [°C]	O-scope Frequency [kHz]	Micro-C Frequency [kHz]	Δ Frequency [kHz]
13	8.77	8.93	0.16
12	8.77	8.93	0.16
	8.62	8.77	0.15
11	8.62	8.77	0.15
10	8.55	8.62	0.07
	8.47		0.15
9	8.55	8.62	0.07
8	8.33	8.47	0.14
7	8.33	8.47	0.14
6	8.33	8.33	0
	8.2		0.13
5	8.2	8.33	0.13
4	8.06	8.2	0.14
3	8.13	8.2	0.07
	8.06		0.14
2	7.94	8.06	0.12
1	7.94	7.94	0
	7.81		0.13
0	7.81	7.81	0
	7.69		0.12
-1	7.69	7.81	0.12
	7.58	7.69	0.11
-2	7.58	7.69	0.11
	7.46	7.58	0.12
-3	7.46	7.58	0.12
	7.35	7.46	0.11
-4	7.46	7.46	0
	7.35		0.11
-5	7.35	7.35	0
	7.25		0.1
-6	7.25	7.25	0
	7.14	7.14	0
	7.04	7.04	0
-7	7.04	7.14	0.1
	6.94	7.04	0.1

-8	6.94	7.04	0.1
		6.94	0
-9	6.85	6.94	0.09
	6.76	6.85	0.09
-10	6.76	6.85	0.09
	6.67	6.76	0.09
-11	6.67	6.67	0
	6.58		0.09
-12	6.58	6.58	0
	6.49	6.49	0
-13	6.41	6.49	0.08
	6.33	6.41	0.08
-14	6.33	6.33	0
	6.25	6.25	0
-15	6.17	6.25	0.08
	6.1	6.17	0.07
		6.1	0
-16	6.1	6.1	0
	6.02	6.02	0
	5.95		0.07
-17	5.95	5.95	0
	5.88	5.88	0
-18	5.81	5.88	0.07
	5.75	5.81	0.06
	5.71	5.75	0.04
-19	5.68	5.68	0
	5.62	5.62	0
-20	5.62	5.62	0
	5.56	5.56	0
	5.49	5.49	0
-21	5.46	5.49	0
	5.43	5.43	0
	5.38	5.38	0
	5.32		0.03
-22	5.32	5.32	0
	5.26	5.26	0
	5.24	5.21	-0.03
	5.21		0
-23	5.15	5.21	0.06
	5.1	5.15	0.05
	5.08	5.1	0.02
	5.05		0.05
-24	5.05	5.05	0

	5	5	0
	4.95	4.95	0
-25	4.95	4.95	0
	4.9	4.9	0
	4.85	4.85	0
	4.81	4.81	0
-26	4.76	4.81	0.08
	4.72	4.76	0.04
	4.67	4.72	0.05
-27	4.67	4.67	0
	4.63	4.63	0
	4.59	4.59	0
	4.55	4.55	0
-28	4.55	4.55	0
	4.5	4.5	0
	4.46	4.46	0
	4.42	4.42	0
-29	4.42	4.42	0
	4.39	4.39	0
	4.35	4.35	0
	4.31		0.04
-30	4.31	4.31	0
	4.27	4.27	0
	4.24	4.24	0
	4.2	4.2	0
	4.17	4.17	0

In Table 4.1.1, it is important to note that there are multiple frequency values for each temperature. As the freezer cooled, multiple frequencies appeared for each temperature, especially if the compressor turned off, causing the temperature to plateau. All of the frequency values recorded during the test are included in Table 4.1.1, arranged in order of greatest to least at the temperature at which they occurred. The column Δ Frequency compares frequency values in the same row. If there is only one frequency value in a row, then it is compared with the frequency value in the previous row of the opposite column.

4.2 Capacitive Sensors Interface Circuit Test

To test the functionality of the proposed circuit, the capacitive sensors were placed upon a digital scale, a VIC-123 scale from Acculab [45][46], and connected to the interface circuitry detailed in section 3.2. Figure 4.2.1 is a photograph of the test setup.

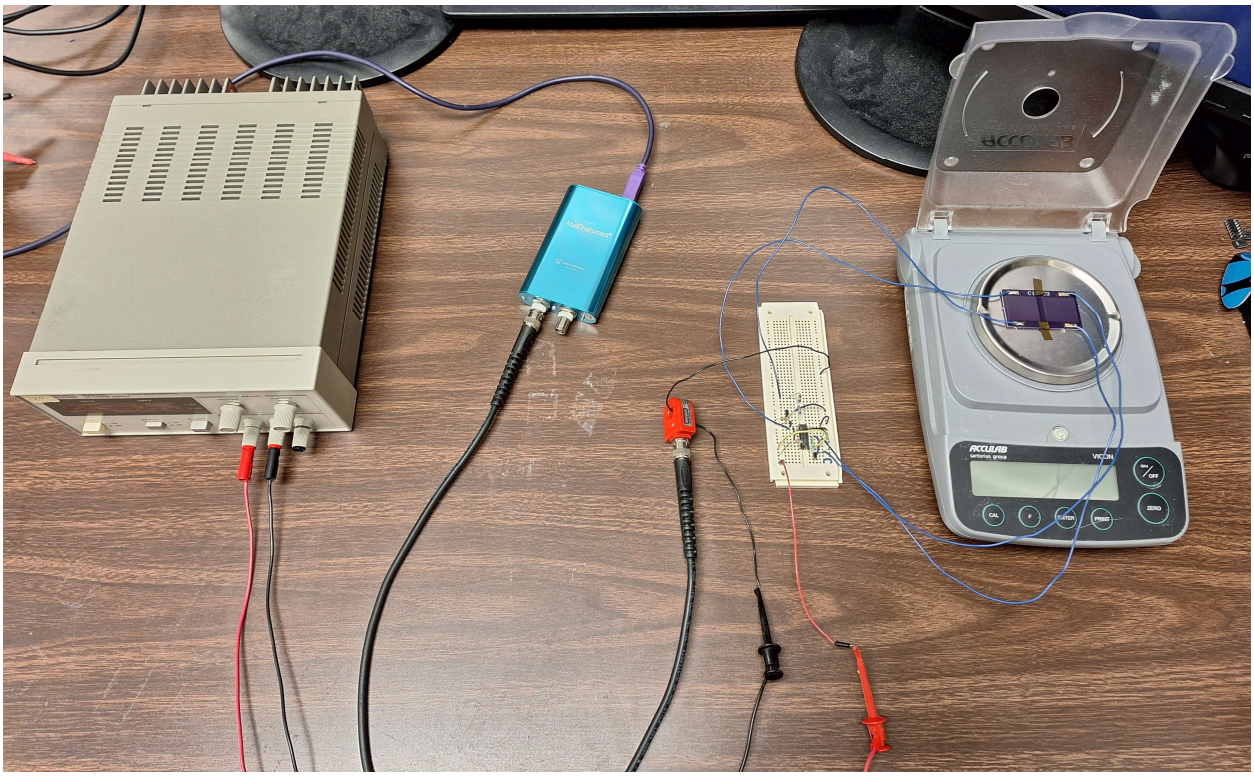

Figure 4.2.1: Capacitive Sensors Interface Circuit Test Setup

Then, the digital oscilloscope was connected to a lab computer and its accompanying software opened. After selecting the FFT option in the software, the scope displayed the frequency spectrum of the oscillation waveform outputted by the current transformer. Additionally, a clean beaker and pipette were fetched, and the beaker was filled with deionized water. Then, drops of deionized water were placed on the surfaces of the capacitive sensors. The presence of the water increased the relative permittivity of the environment of the sensors, which, due to the nature of fringing field sensors discussed in section 2.1, increased their capacitances. The increased capacitances caused a decrease in oscillation frequencies, resulting in a measurable shift in the frequency spectrum displayed on the oscilloscope. By taring the scale before adding each droplet

of water, it was possible to record the water droplet's mass and correlate that to the resultant shift in oscillation frequency.

Figures 4.2.2, 4.2.3, 4.2.4, and 4.2.5 are examples of the frequency spectrum of the oscillation waveform and do not display the frequency spectrums from the test. Each figure is a screenshot of the spectrum analysis of the oscillation waveform as generated by the digital oscilloscope, which does not permit the addition of axes labels or the enlargement of text. In each figure, the x-axis corresponds to frequency, and the y-axis corresponds to relative amplitude, the values of which range between 0 and 1. Figures 4.2.2 and 4.2.3 show the frequency spectrum when there were no water droplets on either sensor. Knowing the designed fundamental frequencies of the oscillators were 10 kHz and 100 kHz allowed for easy location of those corresponding peaks in the frequency spectrum. Figure 4.2.2 shows the cursor at approximately 10 kHz, and Figure 4.2.3 shows the cursor at approximately 100 kHz.

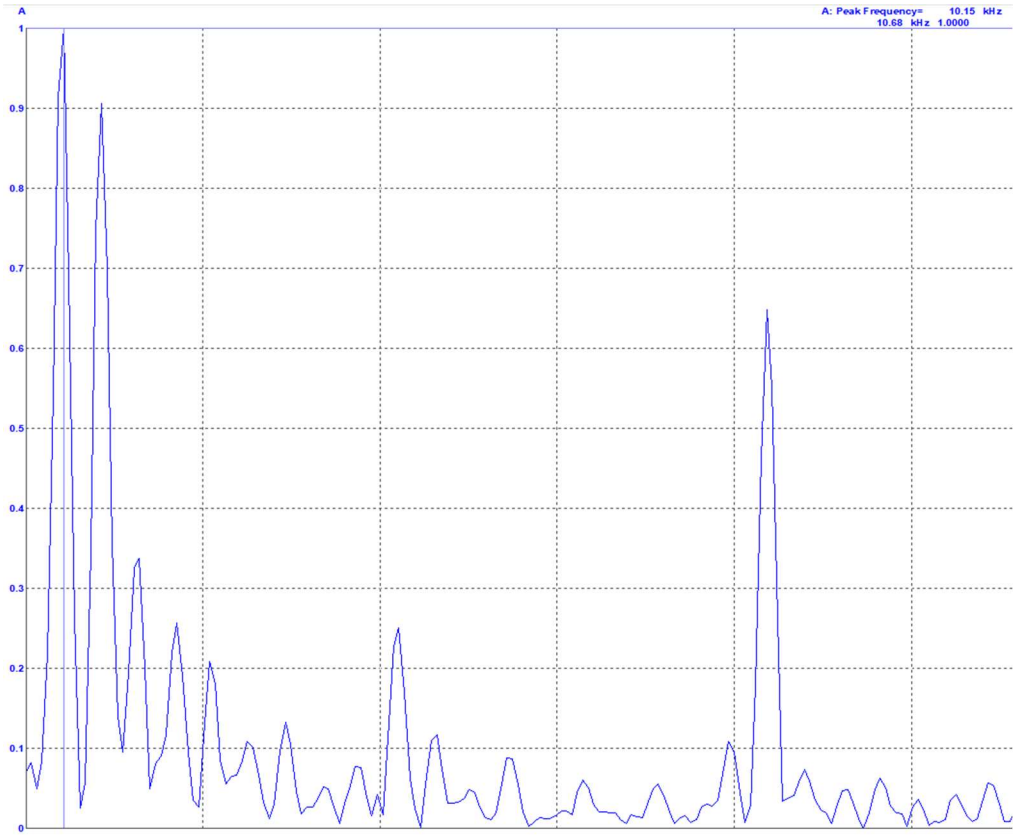

Figure 4.2.2: Spectrum Analysis for Dry Sensors – Cursor on Left Sensor

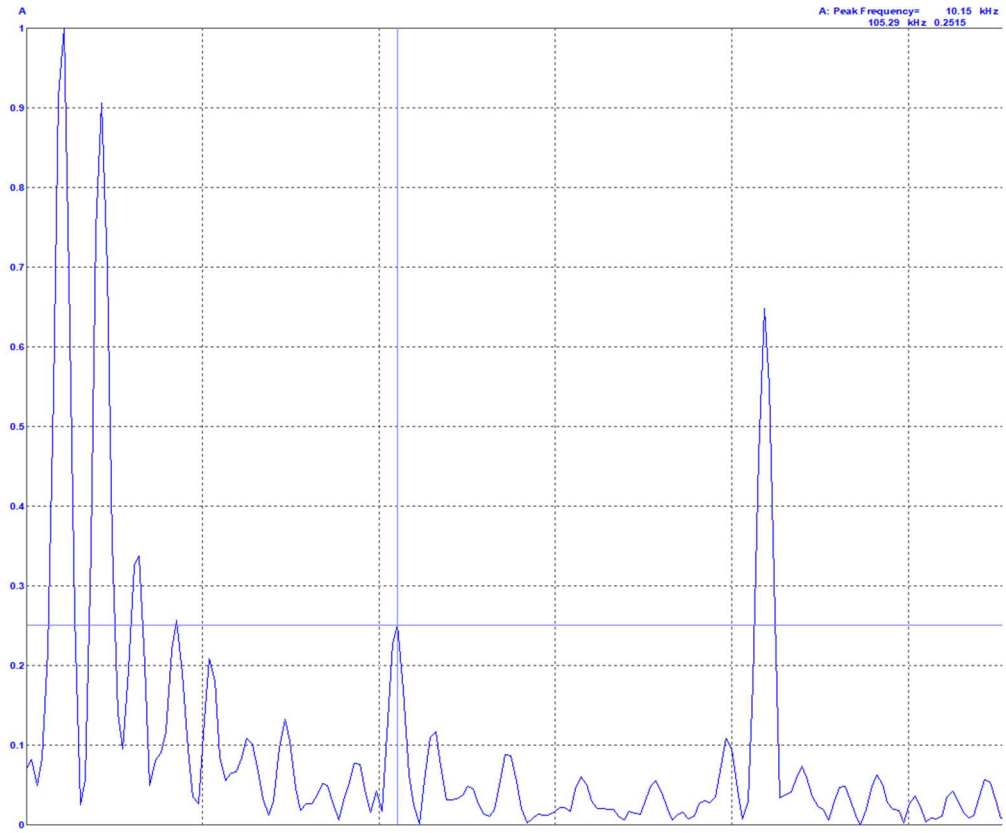

Figure 4.2.3: Spectrum Analysis for Dry Sensors - Cursor on Right Sensor

Figures 4.2.4 and 4.2.5 show the frequency spectrum when there were three water droplets on each sensor. Because added water droplets lowered the frequencies of the oscillators, and the fundamental frequencies (as well as their significant harmonics) were appropriately separated, it was possible to follow the downward shifts of the fundamental frequencies' peaks. Figure 4.2.4 shows the cursor at approximately 7.5 kHz, and Figure 4.2.5 shows the cursor at approximately 56.5 kHz.

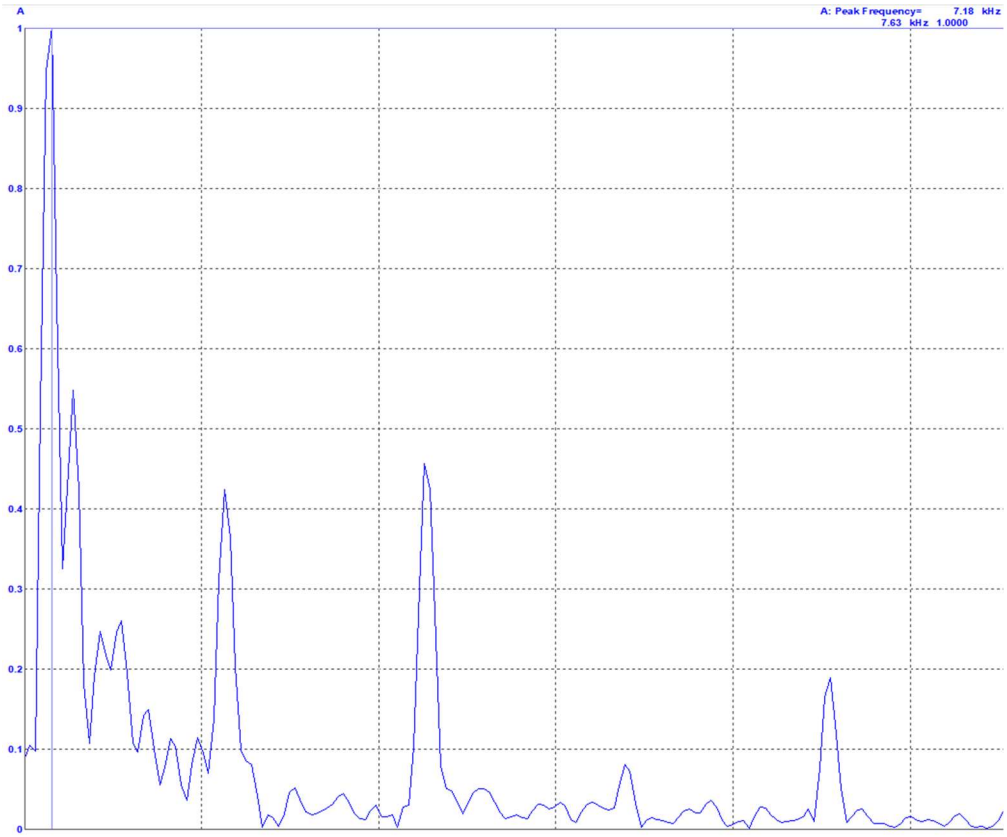

Figure 4.2.4: Spectrum Analysis for Three Water Drops on Sensors - Cursor on Left Sensor

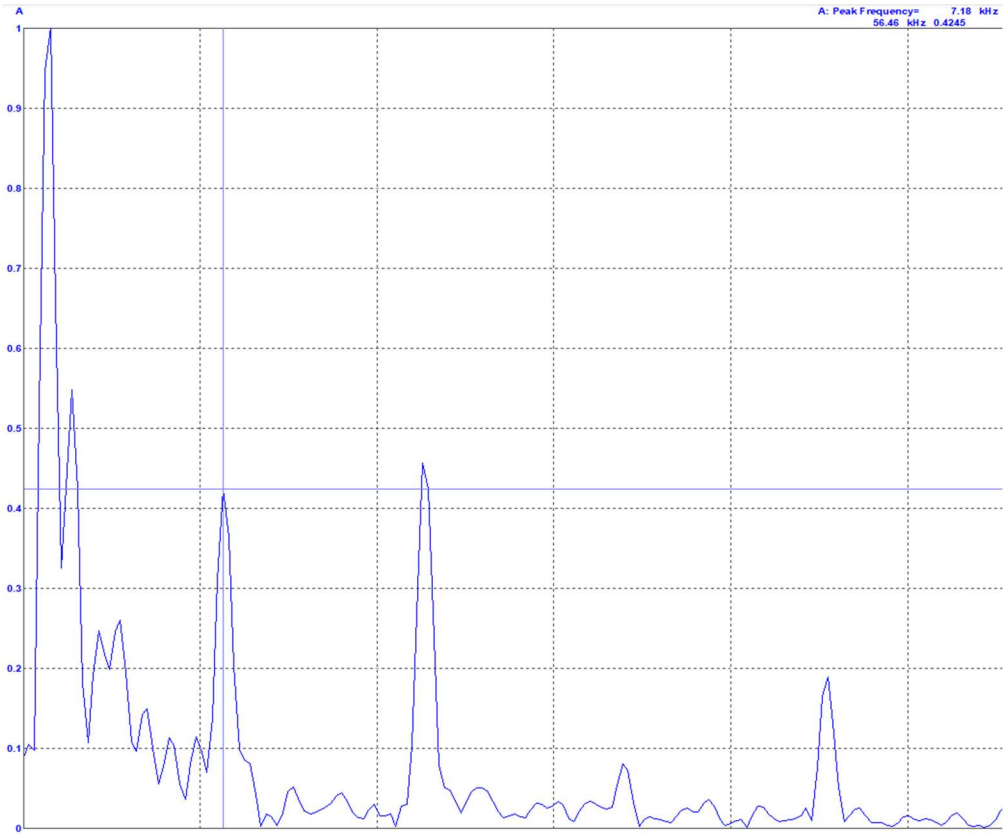

Figure 4.2.5: Spectrum Analysis for Three Water Drops on Sensors - Cursor on Right Sensor

In this manner, the fundamental frequencies of both oscillators were recorded for each water drop added.

For the first iteration, water was only added to the left sensor. That data is presented in Table 4.2.1.

Table 4.2.1: Left Capacitive Sensor Results		
Mass of Water [g]	Frequency [kHz]	Percent Change in Frequencies [%]
0	10.86	-
0.05	8.64	20.44
0.099	7.55	12.62
0.167	6.48	14.17
0.233	5.8	10.49
0.293	5.38	7.24
0.359	4.77	11.34
0.423	4.53	5.03

In the second round of testing, water was only added to the right sensor, and that data is presented in Table 4.2.2.

Table 4.2.2: Right Capacitive Sensor Results		
Mass of Water [g]	Frequency [kHz]	Percent Change in Frequencies [%]
0	111.5	-
0.082	76.4	31.48
0.144	63.3	17.15
0.218	52.3	17.38
0.276	44.1	15.68
0.341	39.6	10.20
0.405	35.8	9.60
0.467	33	7.82

During the third and final stage of the test, water was added to both sensors. A drop was added to the left sensor, its mass recorded, and the frequencies of both oscillators recorded. Then, a drop was added to the right sensor, its mass recorded, and the frequencies of both oscillators recorded. Those results are shown in Table 4.2.3.

Table 4.2.3: Both Capacitive Sensors Results					
Mass of Water – Left [g]	Mass of Water – Right [g]	Frequency – Left [kHz]	Frequency – Right [kHz]	Percent Change in Left Frequencies [%]	Percent Change in Right Frequencies [%]
0	0	10.73	111.45	-	-
0.048	0	8.94	111.45	16.68	0
0.048	0.053	8.94	88.06	0	20.99
0.104	0.053	7.7	87.78	13.87	0.32
0.104	0.11	7.7	72.37	0	17.56
0.145	0.11	7.15	71.82	7.14	0.76
0.145	0.161	7.15	63.7	0	11.31
0.217	0.161	6.33	63.43	11.47	0.42
0.217	0.239	6.33	55.59	0	12.36
0.282	0.239	5.64	54.76	10.90	1.49
0.282	0.31	5.64	46.37	0	15.32
0.343	0.31	5.09	45.95	9.75	0.91
0.343	0.388	5.09	42.51	0	7.49

0.405	0.388	4.68	41.55	8.06	2.26
0.405	0.441	4.68	38.66	0	6.96

It should be noted that the equation used to calculate the percent change in frequency is given as

$$Percent\ Change = 100 \times \frac{(Measured\ Frequency - Previous\ Frequency)}{Previous\ Frequency}. \qquad (4.2.1)$$

Chapter 5

Data Analysis

5.1 Thermistor Test Data Analysis

In Figure 5.1.1, the frequencies as measured by the oscilloscope and microcontroller are plotted versus temperature in Kelvin.

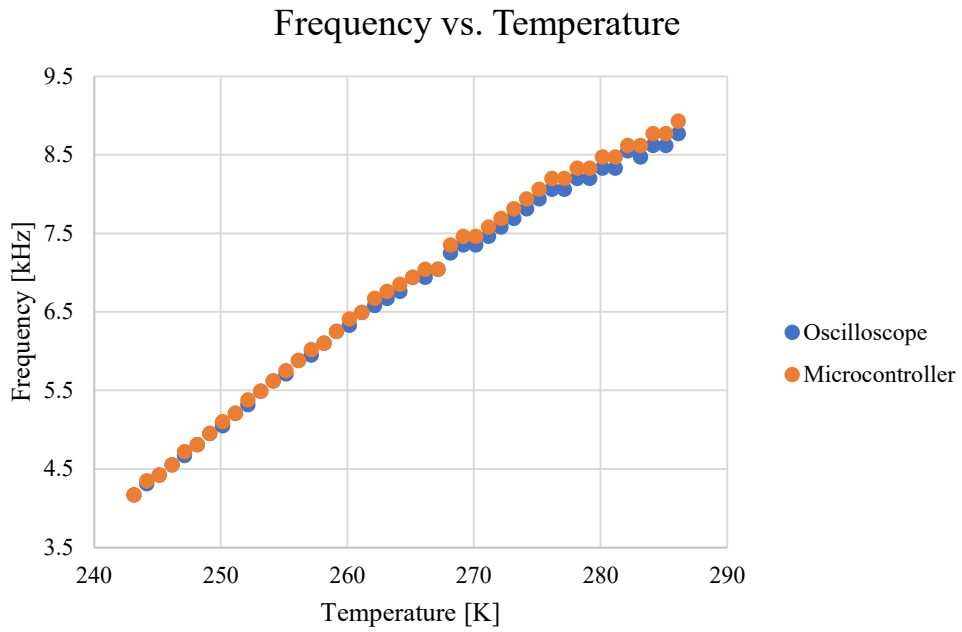

Figure 5.1.1: Thermistor Frequency vs. Temperature Data

In Figure 5.1.1, the frequency values used for both the oscilloscope and the microcontroller are the lowest values recorded for each temperature in Table 4.1.1. As shown in the graph, the microcontroller measurements follow those of the oscilloscope closely; the largest difference in measured frequency was 160 Hz at 13 °C. Figure 5.1.2 is a graph of the frequencies measured by the microcontroller versus temperature.

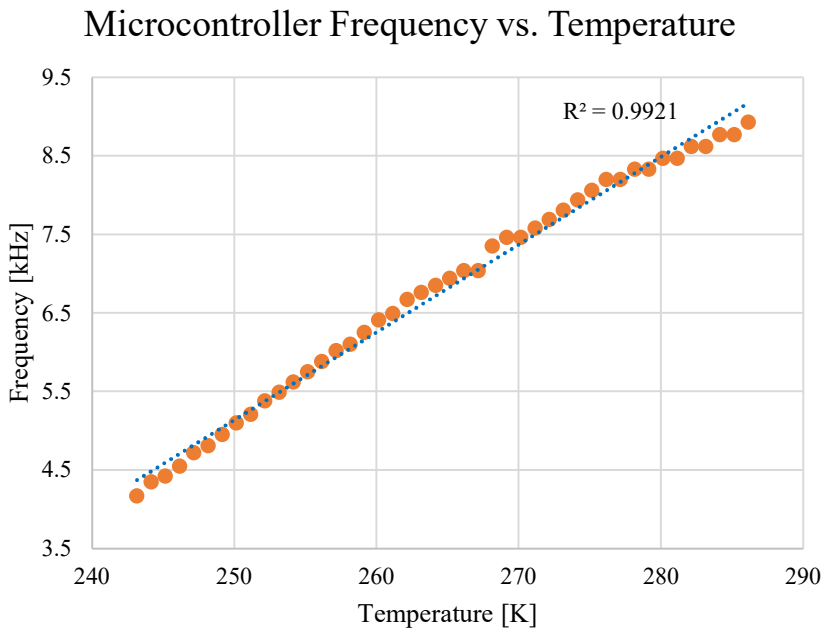

Figure 5.1.2: Thermistor Frequency vs. Temperature Microcontroller Data (Figure adapted from Figure 13 "A plot of the measured frequency vs. freezer temperature" [15])

The frequencies measured by the microcontroller demonstrate a marked linearity, as shown by the R^2 value of 0.9921. Because of the physical nature of the experiment, there is noise present in the data that warps it from a purely linear trend. That noise is the result of a plethora of causes, such as limited resolution of the microcontroller or stray capacitances created by breadboarded connections.

5.2 Capacitive Sensors Test Data Analysis

Figure 5.2.1 is a graph of the data from Table 4.2.1.

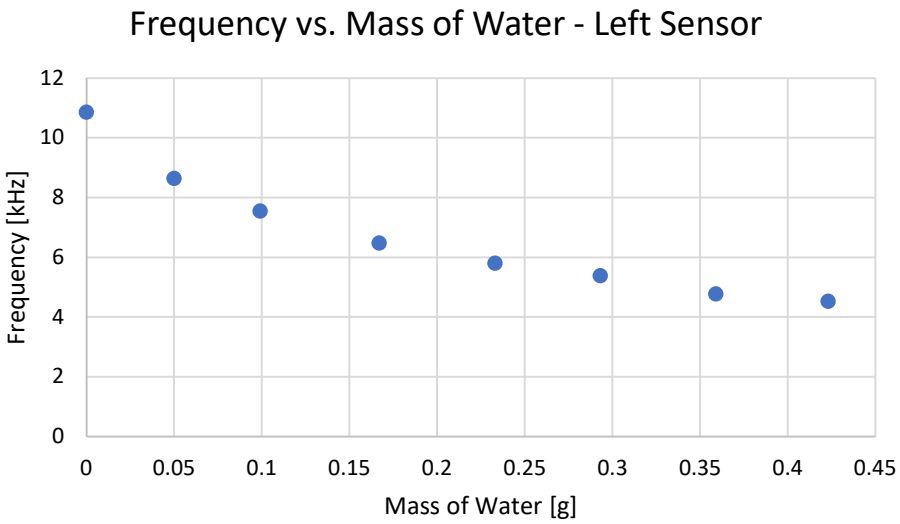

Figure 5.2.1: Left Capacitive Sensor Frequency vs. Mass of Water

Figure 5.2.2 is a graph of the data from Table 4.2.2.

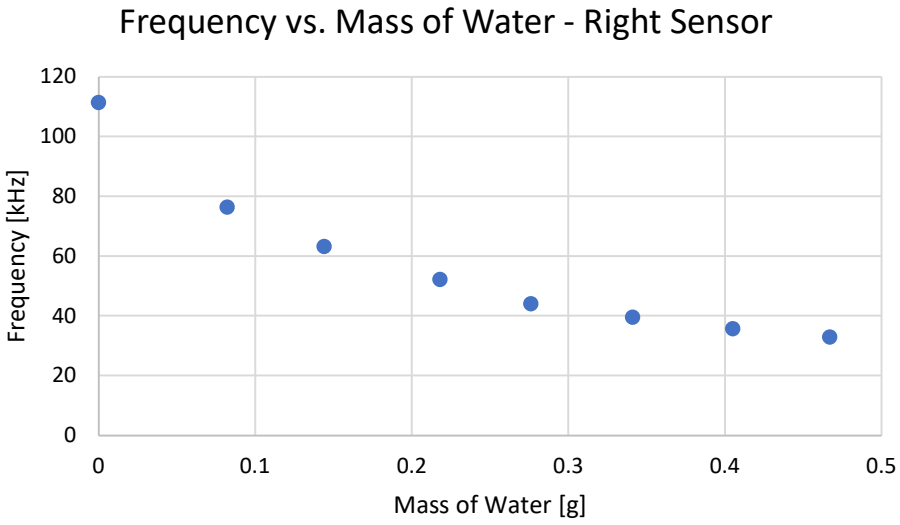

Figure 5.2.2: Right Capacitive Sensor Frequency vs. Mass of Water

Lastly, Figure 5.2.3 is a graph of the data from Table 4.2.3.

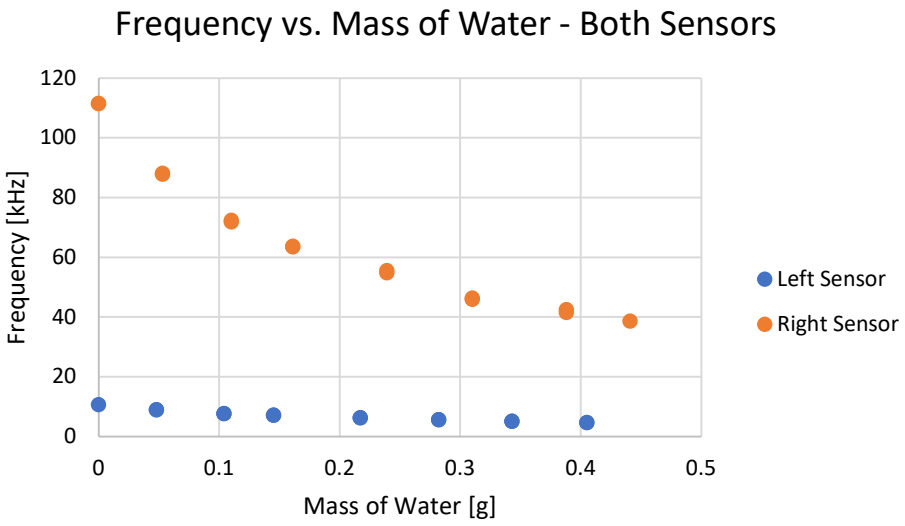

Figure 5.2.3: Capacitive Sensors Frequency vs. Mass of Water

The frequency values measured during the test of both sensors are consistent with those measured during the tests of the individual sensors.

Overall, the right sensor demonstrated greater sensitivity, found by examining the percent changes in frequencies for both sensors. For its individual test, the data of which is shown in Table 4.2.1, the left sensor had an average percent change of 11.62%. The right sensor, however, had an average percent change of 15.62% for its individual test, the data of which is shown in Table 4.2.2. For the combined test, the data of which is shown in Table 4.2.3, the left sensor had an average percent change of 11.12% for each water drop added while the right sensor had an average percent change of 13.14% for each water drop added. As a note for the sake of clarity, the average percent change of the right sensor for the combined test does not account for the small percent changes that occurred when water was added to the left sensor; those changes are discussed in the following paragraph. The right sensor, on average, experienced a larger percent change in frequency for each water drop added than the left sensor; therefore, the right sensor demonstrated greater sensitivity than the left sensor.

During the test of both sensors, frequency shifts for the oscillator of the left sensor were only observed when water was added to the sensor's surface. However, frequency shifts for the oscillator connected to the right sensor were observed both when water was added to the sensor's surface and when water was added to the surface of the left sensor. When water was added to the right sensor, the average amount of frequency shift measured for the right sensor was 9.93 kHz, with an associated average percent change of 13.14%. When water was added to the left sensor, the average amount of frequency shift measured for the right sensor was 473 Hz, with an associated average percent change of 0.88%. A possible explanation for the unexpected shifts is the spreading of the water drop over the sensor's surface. After a water drop was placed on the sensor' surface, it spread a small amount until it reached the limits defined by surface tension. After it spread to its limits, the water drop covered more surface area of the sensor than it did when initially added, which caused the small frequency shift. As the right sensor was more sensitive than the left sensor, it is plausible that the right sensor's measurements reflected the small frequency shifts when the left sensor was unable to detect them.

Chapter 6

Conclusion and Future Work

In conclusion, the proposed interface circuits accurately interpret sensor measurements and demonstrate proper functionality with a modicum of error. The interface circuit fabricated for the thermistor produces frequency readings that compare favorably with frequency readings taken by a standard oscilloscope, with a maximum error between frequency readings of 160 Hz. The interface circuit designed for the dual capacitive sensors demonstrates reliability through repeated testing and also produces frequency data that conforms with expected effects of adding water droplets to the sensors' surfaces. The successful operation of both circuits demonstrates the viability of modulating the sensor signal onto the power supply current and later recovering it, limiting the needed circuit connections to dual power/ground connections. However, both interface circuits still present areas for further development.

Future areas of work on these projects are manifold. For the thermistor interface circuit, it may be intriguing to adjust the fixed capacitance value so as to raise the frequency of oscillation to its highest possible value at room temperature, which will result in greater sensitivity to decreasing temperatures. Additionally, there is potential for the microcontroller code to be refined so as to produce a useful result for an end user. Currently, the microcontroller only outputs the measured frequency of the oscillator, but with some addition and modification, it might be able to display temperature for a user, converting the entire circuit into a thermometer. For the capacitive sensor circuit, it might be useful to convert the relaxation oscillator portion into a PCB to remove potential sources of error from unstable breadboard connections. And, the streamlining of data analysis is another area of possible improvement. Encoding the spectrum analysis and frequency measurement and relating those frequency values to moisture levels that

are then output to the user will produce a more user-friendly circuit. In summary, the interface circuits demonstrate initial success and offer many avenues for improvement and further research.

References

[1] R. N. Dean et al., "Characterization and Experimental Verification of the Nonlinear Distortion in a Technique for Measuring the Relative Velocity Between Micromachined Structures in Normal Translational Motion," in IEEE Sensors Journal, vol. 7, no. 4, pp. 496-501, April 2007, doi: 10.1109/JSEN.2007.891920.

[2] R.N. Dean and F.T. Werner, “A PCB environmental sensor for use in monitoring drought conditions in estuaries,” J. of Microelectronics and Electronic Packaging, vol. 13, 2016, pp. 182-187.

[3] R. N. Dean and M. A. Previti, "Passive Wireless Instrumented Getter," in IEEE Sensors Letters, vol. 7, no. 8, pp. 1-4, Aug. 2023, Art no. 4501604, doi: 10.1109/LSENS.2023.3297794.

[4] S.M. Wentworth, *Applied Electromagnetics*. Hoboken, NJ, USA: John Wiley & Sons, Inc., 2007.

[5] C. G. Malmberg and A. A. Maryott, “Dielectric Constant of Water from 0° to 100° C,” in Journal of Research of the National Bureau of Standards, vol. 56, no. 1, January 1956.

[6] S. S. Stuchly, G. Gajda, L. Anderson and A. Kraszewski, “A new sensor for dielectric measurements,” in IEEE Transactions on Instrumentation and Measurement, vol. IM-35, no. 2, pp. 138-141, June 1986, doi: 10.1109/TIM.1986.6499079.

[7] K. P. A. P. Esselle and S. S. Stuchly, “Capacitive sensors for in-vivo measurements of the dielectric properties of biological materials,” in IEEE Transactions on Instrumentation and Measurement, vol. 37, no. 1, pp. 101-105, March 1988, doi: 10.1109/19.2675.

[8] S. Aoyagi and Yu-Chong Tai, “Development of surface micromachinable capacitive accelerometer using fringe electrical field,” TRANSDUCERS ‘03. 12th International

Conference on Solid-State Sensors, Actuators and Microsystems. Digest of Technical Papers (Cat. No.03TH8664), Boston, MA, USA, 2003, pp. 1383-1386 vol.2, doi: 10.1109/SENSOR.2003.1217032.

[9] R. N. Dean, A. Rane, M. Baginski, Z. Hartzog and D. J. Elton, "Capacitive fringing field sensors in printed circuit board technology," 2010 IEEE Instrumentation & Measurement Technology Conference Proceedings, Austin, TX, USA, 2010, pp. 970-974, doi: 10.1109/IMTC.2010.5488058.

[10] R. B. McIntosh and M. E. Casada, "Fringing Field Capacitance Sensor for Measuring the Moisture Content of Agricultural Commodities," in IEEE Sensors Journal, vol. 8, no. 3, pp. 240-247, March 2008, doi: 10.1109/JSEN.2007.913140.

[11] Y. -T. Li, Y. -L. Tzeng, C. -M. Chao and K. Wang, "Electrode design optimization of a CMOS fringing-field capacitive sensor," 2012 7th IEEE International Conference on Nano/Micro Engineered and Molecular Systems (NEMS), Kyoto, Japan, 2012, pp. 603-606, doi: 10.1109/NEMS.2012.6196848.

[12] R. N. Dean, J. D. Craven, E. A. Guertal and K. A. Varnavas, "A PCB Sensor for Status Monitoring of Stored Food Stocks," in IEEE Sensors Letters, vol. 3, no. 4, pp. 1-4, April 2019, Art no. 6000604, doi: 10.1109/LSENS.2019.2902837.

[13] S. Malik, L. Somappa, M. Ahmad, S. Sonkusale and M. S. Baghini, "A Fringing Field Based Screen-Printed Flexible Capacitive Moisture and Water Level Sensor," 2020 IEEE International Conference on Flexible and Printable Sensors and Systems (FLEPS), Manchester, UK, 2020, pp. 1-4, doi: 10.1109/FLEPS49123.2020.9239552.

[14] S. Das and B. Chakraborty, "A Pencil Drawn Capacitive Sensor used for Liquid Drug Volume Measurement in Syringe Pump," 2020 IEEE Applied Signal Processing

Conference (ASPCON), Kolkata, India, 2020, pp. 85-88, doi: 10.1109/ASPCON49795.2020.9276687.

[15] E.C. Hatfield, M.A.R. Kreitzer and R.N. Dean, “2-Wire Relaxation Oscillator Sensor Interface Circuit,” IEEE Trans. on Instrumentation & Measurement, submitted 7/25/23, 7pp.

[16] R. N. Dean and A. K. Rane, "A Digital Frequency-Locked Loop System for Capacitance Measurement," in IEEE Transactions on Instrumentation and Measurement, vol. 62, no. 4, pp. 777-784, April 2013, doi: 10.1109/TIM.2013.2240092.

[17] G. K. Kostopoulos, "Design and analysis nomograms for pulse-width and frequency modulation using the 555 Timer," in IEEE Circuits & Systems Magazine, vol. 6, no. 2, pp. 4-11, June 1984, doi: 10.1109/MCAS.1984.6323930.

[18] A. Cichocki and R. Unbehauen, "A switched-capacitor interface for capacitive sensors based on relaxation oscillators," in IEEE Transactions on Instrumentation and Measurement, vol. 39, no. 5, pp. 797-799, Oct. 1990, doi: 10.1109/19.58630.

[19] M. H. Splithof, A. J. M. van Tuijl, S. L. J. Gierkink and E. A. M. Klumperink, "Current-ratio temperature compensation in bipolar relaxation oscillator," Proceedings of the 24th European Solid-State Circuits Conference, The Hague, Netherlands, 1998, pp. 392-395, doi: 10.1109/ESSCIR.1998.186291.

[20] Yili Liu, Song Chen, M. Nakayama and K. Watanabe, "Limitations of a relaxation oscillator in capacitance measurements," in IEEE Transactions on Instrumentation and Measurement, vol. 49, no. 5, pp. 980-983, Oct. 2000, doi: 10.1109/19.872917.

[21] U. Denier, "Analysis and Design of an Ultralow-Power CMOS Relaxation Oscillator," in IEEE Transactions on Circuits and Systems I: Regular Papers, vol. 57, no. 8, pp. 1973-1982, Aug. 2010, doi: 10.1109/TCSI.2010.2041504.

[22] S. -B. Huang, J. -G. Chen, F. Yang and Y. -H. Cheng, "Design of an ultralow-power CMOS relaxation oscillator for piezoresistive pressure sensor," 2012 IEEE 11th International Conference on Solid-State and Integrated Circuit Technology, Xi'an, China, 2012, pp. 1-3, doi: 10.1109/ICSICT.2012.6467878.

[23] T. Islam, S. A. Khan, M. F. A. Khan and S. C. Mukhopadhyay, "A Relaxation Oscillator-Based Transformer Ratio Arm Bridge Circuit for Capacitive Humidity Sensor," in IEEE Transactions on Instrumentation and Measurement, vol. 64, no. 12, pp. 3414-3422, Dec. 2015, doi: 10.1109/TIM.2015.2459473.

[24] Y. Wang, L. Rong, L. Xie, J. Liu and G. Wen, "A 255nW 138kHz RC oscillator for ultra-low power applications," 2016 IEEE MTT-S International Wireless Symposium (IWS), Shanghai, China, 2016, pp. 1-4, doi: 10.1109/IEEE-IWS.2016.7585431.

[25] W. Zhou, W. L. Goh and Y. Gao, "Integrated Temperature Sensor with CMOS Relaxation Oscillator Based Sensor Interface for Biomedical Sensing," 2019 Electron Devices Technology and Manufacturing Conference (EDTM), Singapore, 2019, pp. 416-418, doi: 10.1109/EDTM.2019.8731231.

[26] Oshpark. https://oshpark.com/ (accessed October 19, 2023).

[27] “NTC SMD Thermistors,” Kyocera.

[28] “MC14049UB,” Semiconductor Components Industries, LLC, MC14049UB/D, 2022.

[29] Y. Meng and R. N. Dean, "A Technique for Improving the Linear Operating Range for a Relative Phase Delay Capacitive Sensor Interface Circuit," in IEEE Transactions on

Instrumentation and Measurement, vol. 65, no. 3, pp. 624-630, March 2016, doi: 10.1109/TIM.2015.2507698.

[30] “ZVN4306G,” Diodes, Inc., DS33369 Rev. 5 – 2, 2022.

[31] “HP E361XA 30W BENCH SERIES DC POWER SUPPLIES,” Hewlett Packard, 5959-5304, 1992.

[32] E. Rodríguez-Schwendtner, M. -C. Navarrete, N. Díaz-Herrera, A. González-Cano and Ó. Esteban, "Advanced Plasmonic Fiber-Optic Sensor for High Sensitivity Measurement of Magnetic Field," in IEEE Sensors Journal, vol. 19, no. 17, pp. 7355-7364, 1 Sept.1, 2019, doi: 10.1109/JSEN.2019.2916157.

[33] “CT Current Transformer,” Bergoz.

[34] P. Craievich, C. Bontoiu, G. Ciani and M. Ferianis, "Trapped modes analysis for the elettra booster DCCT installation," 2007 IEEE Particle Accelerator Conference (PAC), Albuquerque, NM, USA, 2007, pp. 3970-3972, doi: 10.1109/PAC.2007.4439944.

[35] “Agilent E3631A Triple Output DC Power Supply,” Agilent Technologies, Inc., Budd Lake, NJ, USA, KIO_10-32.11.24, 2003.

[36] “LT1220,” Linear Technology Corp., Milpitas, CA, USA, 1220fb LT/CP 0801 1.5K, 1991.

[37] A. N. Beal et al., "Design and simulation of a high frequency exact solvable chaotic oscillator," MILCOM 2012 - 2012 IEEE Military Communications Conference, Orlando, FL, USA, 2012, pp. 1-6, doi: 10.1109/MILCOM.2012.6415803.

[38] “LM339B, LM2901B, LM339, LM239, LM139, LM2901 Quad Differential Comparators,” Texas Instruments, Dallas, TX, USA, SLCS006X, 2023.

[39] A. S. Vyas, R. Radha and Y. K. Bharath, "Development of Electrical Fence Energizet for a Farm Fencing System," 2018 4th International Conference for Convergence in

Technology (I2CT), Mangalore, India, 2018, pp. 1-6, doi: 10.1109/I2CT42659.2018.9058070.

[40] “MC14013B,” Semiconductor Components Industries, LLC, Denver, CO, USA, MC14013B/D, 2014.

[41] “Photon Datasheet,” Particle, 2023.

[42] V. K. K, A. P, C. A, G. K. K and K. Deepthi, "IoT Detection based Energy Meter Integrated with Smart Devices," 2023 Second International Conference on Electronics and Renewable Systems (ICEARS), Tuticorin, India, 2023, pp. 556-559, doi: 10.1109/ICEARS56392.2023.10085200.

[43] “ZVN4306AV,” Zetek, Chadderton, Oldham, UK, 1997.

[44] “VT DSO-2810 Manual,” Virtins Technology, 2017.

[45] “ACCULAB VICON,” Acculab, WVI6006-p05071, 2005.

[46] R. E. Dean and R. N. Dean, "EC Sensor to Improve Sea Turtle Nesting Research," 2022 IEEE Sensors, Dallas, TX, USA, 2022, pp. 1-4, doi: 10.1109/SENSORS52175.2022.9967211.

Appendix A

Microcontroller Code:

```
// Hatfield, Emily
// Purpose: Read Frequency of amplified Current Transformer (CT) output
// Created: 9 November 2021
// Last Edited: 16 May 2023

#include "math.h"

const int CTAmp = A0; // Input Pin to read signal from op-amp circuit

float cycleLow = 0; // Signal low pulse width
float CTAmpPeriod = 0; // Signal period
float CTAmpFrequency = 0; // Signal frequency

SerialLogHandler logHandler; // Set up serial communication

void setup() {
  /* Set up Input and Output pins */
  pinMode(CTAmp, INPUT_PULLDOWN); // Set up input pin with pulldown resistor
}

void loop() {
  /* PulseIn attempt */

  cycleLow = pulseIn(CTAmp, LOW); // Measure low pulse width

  CTAmpPeriod = cycleLow * 2;

  CTAmpPeriod = 0.000001 * CTAmpPeriod; // Convert period to seconds from microseconds

  CTAmpFrequency = 1 / CTAmpPeriod; // Calculate signal frequency

  Serial.printlnf("Frequency = %f", CTAmpFrequency); // Print frequency value via serial
connection
  Particle.publish("Frequency", String::format("%f", CTAmpFrequency)); // Publish frequency
value via WiFi

  delay(1000); // Delay 1 second
}
```

Appendix B

Virtins DSO-281OR Tutorial:

The Virtins DSO-281OR is a digital oscilloscope designed for use with a computer. Figure B.1 is a photo of the oscilloscope.

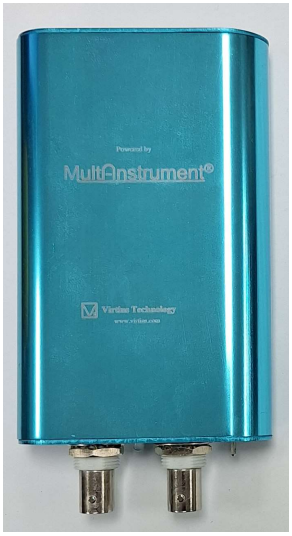

Figure B.1: Virtins DSO-281OR

The oscilloscope has three connection points: two BNC connectors on the front and a USB connector on the back. Each BNC connector is a signal input and is labeled as either Channel A or Channel B. The USB connector is the oscilloscope's input/output connection to the computer, supplying power to the oscilloscope as well as communicating data between the oscilloscope and the computer.

In order to use the Virtins DSO-281OR, it is necessary to run the Virtins Multi-Instrument software on the computer connected to the oscilloscope. Once the software is launched, it will open a window similar to Figure B.2.

Figure B.2: Multi-Instrument Oscilloscope Display

This window is the main control panel for the oscilloscope as well as its display. The controls are located along the top and bottom of the screen, and the display fills the space between the controls.

At the top of the screen are the tabs File, Setting, Instrument, Window, and Help. File allows the user to handle data files in various ways, such as importing and exporting them. Setting provides access to detailed control panels for the oscilloscope and the display, which are useful for altering parameters not found among the options on the main panel. Setting also provides the ability to save control panel settings for future use. Instrument shows the available functions for signal processing, including an oscilloscope, spectrum analyzer, multimeter, and signal generator; selecting a function adds its respective window to the display, and deselecting a function closes its respective window. Window adjusts the organization of the different windows in the display. Lastly, Help provides access to the user manuals for the DSO-281OR and Multi-Instrument.

Below the tabs is the first line of the control panel. At the very left is an open folder icon, which loads previously saved signals into the display when the oscilloscope is not actively running. The floppy disk icon to the right of the open folder icon saves signals and also requires the oscilloscope to not be actively running. To the right of those two icons is the word “Trigger” followed by 6 alterable parameters, which control the trigger settings (eg. to which channel the trigger is attached). Following the trigger parameters is the word “Sample” followed by 2 alterable parameters, which control the rate of sampling and the channels sampled. At the end of the row are two buttons, “Record” and “Auto”. Clicking “Record” records the data on the channels being sampled; the oscilloscope must not be actively running to begin recording. Clicking “Auto” auto-scales the windows in the display to the best settings (as determined by the computer) for viewing the input signals.

Beneath the first line of the control panel is the second line of the control panel. At the very left is a red/green circle icon, which controls whether the oscilloscope is actively running or not. After the circle icon are four rectangular icons, each displaying a different picture. These four icons correspond to the different functions listed under the Instrument tab; clicking an icon adds or removes its window from the display. To the right of the four function icons are seven more icons. The first icon, which appears as an upside down glass, inverts the signals. The second and third icons, which display either the letter “A” or “B” to the right of a perpendicular, zero the signal on the labeled channel. The fourth, fifth, sixth, and seventh icons are all useful for the recording and replaying of signals. Following the seven icons are four alterable parameters that control the coupling and scale of each channel. Each parameter is color-coded to match the displayed signal of the channel to which it corresponds. Finally, the word “Probe” appears,

followed by two alterable parameters. These parameters account for the impedance of the probes used.

The third control line appears at the bottom of the screen beneath the display. It contains parameters concerning the current active window in the display (i.e. the window in which the mouse has most recently been clicked). For example, if the oscilloscope window has most recently been selected, then the parameters available allow the user to alter items such as the scales for both axes of the oscilloscope graph.

The display portion of the program, located between the lines of controls, contains the windows of all currently active functions. In each window, values of significance (eg. the maximum and minimum amplitudes in the oscilloscope graph) are displayed at the top of the graph, centered and color-coded. The y-axis scale for channel A is displayed on the left side of the graph, and the y-axis scale for channel B is displayed on the right side of the graph. In order to zoom in or out on the graph, it is necessary to zoom in or out on the axes of the graph. To accomplish that, the mouse must be located over the axis in question; when it is properly located, the mouse icon will change to a magnifying glass to the right of a plus sign. Zooming in corresponds to left clicking with the mouse, and zooming out corresponds to right clicking with the mouse. Within the confines of the graph itself, clicking the mouse creates a cursor and displays the coordinates of the datapoints of both signals that are nearest to where the mouse was clicked at the top of the window. Holding down the left mouse button enables the user to drag the cursor to any desired point. In order to affix the cursor at a desired location, the user must double-click to place the cursor on channel A or double-click while pressing “Ctrl” on the keyboard to place the cursor on channel B. A second stationary cursor may be placed by pressing

"Shift" on the keyboard in addition to the actions previously described. The coordinates of both cursors as well as the differences between the coordinates are displayed at the top of the window.